Review

New Roles Assigned to the α_1–β_1 (and α_2–β_2) Interface of the Human Hemoglobin Molecule from Physiological to Cellular

Yoshiaki Sugawara *, Mai Yamada, Eriko Ueno, Mai Okazaki, Aya Okamoto, Mariko Miyake, Fusako Fukami and Ai Yano

Department of Health Science, Prefectural University of Hiroshima, Hiroshima 734-8558, Japan;
E-Mails: m-yamada88428@pref.hiroshima.lg.jp (M.Y.); eriko.u-everblue@cup.ocn.ne.jp (E.U.);
okazaki-mai@mitsui-hanbai.co.jp (M.O.); ayaozaki0209@gmail.com (A.O.);
happysmile1024@power.odn.ne.jp (M.M.); 6030vkzf@jcom.home.ne.jp (F.F.);
a-nishino@afs.or.jp (A.Y.)

* Author to whom correspondence should be addressed; E-Mail: sugawara@pu-hiroshima.ac.jp;
 Tel.: +81-82-251-9783; Fax: +81-82-251-9405.

Abstract: Cellular life is reliant upon rapid and efficient responses to internal and external conditions. The basic molecular events associated with these processes are the structural transitions of the proteins (structural protein allostery) involved. From this view, the human hemoglobin (Hb) molecule ($\alpha_2\beta_2$) holds a special position in this field. Hb has two types of $\alpha\beta$ interface (*i.e.*, $\alpha_1\beta_1$ [and $\alpha_2\beta_2$] and $\alpha_1\beta_2$ [and $\alpha_2\beta_1$]). The latter α_1–β_2 (and α_2–β_1) interface is known to be associated with cooperative O_2 binding, and exhibits principal roles if the molecule goes from its deoxy to oxy quaternary structure. However, the role of the former α_1–β_1 (and α_2–β_2) interface has been unclear for a long time. In this regard, important and intriguing observations have been accumulating. A new role was attributed first as stabilizing the HbO_2 tetramer against acidic autoxidation. That is, the α_1–β_1 (and α_2–β_2) interface produces a conformational constraint in the β chain whereby the distal (E7) histidine (His) residue is tilted slightly away from the bound O_2 so as to prevent proton-catalyzed displacement of O_2^- by a solvent water molecule. The β chains thus acquire pH-dependent delayed autoxidation in the HbO_2 tetramer. The next role was suggested by our studies searching for similar phenomena in normal human erythrocytes under mild heating. Tilting of the distal (E7) His in turn triggered degradation of the Hb molecule to hemichrome, and subsequent clustering of Heinz bodies within the erythrocyte.

As Heinz body-containing red cells become trapped in the spleen, it was demonstrated that the α_1–β_1 (and α_2–β_2) interface may exert delicate control of the fate (removal) of its own erythrocyte. Herein we review and summarize the related results and current interpretation of the oxidative behavior of human Hb, emphasizing the correlation between hemichrome emergence and Heinz-body formation, and specifically discuss the new roles assigned to the α_1–β_1 (and α_2–β_2) interface. The α_1–β_1 (and α_2–β_2) interface seems to adequately differentiate between the two types of function (dual roles) from physiological to cellular.

Keywords: hemoglobin; α_1–β_1 (and α_2–β_2) interface; pH-dependent biphasic autoxidation; temperature-dependent hemichrome formation; Heinz-body clustering

1. Introduction

In erythrocytes *in situ*, the reaction dynamics of human hemoglobin (Hb) with molecular dioxygen (O_2) make them a particularly suitable O_2 carrier. Hb can bind O_2 in the ferrous form to carry out its physiological functions. During this reversible O_2 binding, the oxygenated form of Hb (HbO_2) is known to be oxidized by the bound O_2 to the ferric met form (metHb), which cannot be oxygenated, and is thus physiologically inactive. However, the content of metHb in normal red cells *in situ* has been reported to be $\leq 1\%$ [1,2]. An intra-erythrocytic nicotinamide adenine dinucleotide (NADH)-dependent reducing system can reduce metHb to deoxy-ferrous Hb and prevent the continued accumulation of metHb resulting from oxidation of the bound O_2 to the ferrous heme iron(II) [3-5]. Even so, it has been suggested that its oxidation (autoxidation) process can be followed by transformation of the oxidized molecule (high-spin Fe^{3+}) into a species absorbing as a low-spin compound, *i.e.*, hemichrome, the formation of which can result in the accumulation of soluble and insoluble hemichromes and precipitation [6-11]. Despite these findings, direct evidence of hemichrome formation in normal erythrocytes is lacking.

Since the early works of Brooks [12,13], the oxidative process (autoxidation) of human Hb (HbO_2) has been investigated by several workers. Among others, Monsouri and Winterhalter [14] and Tomoda *et al.* [15] observed that the rate of autoxidation is strongly dependent upon the pH values of solutions. The study of Monsouri and Winterhalter [14] also showed that autoxidation of human HbO_2 exhibited a biphasic nature with a initial fast (k_A^f) reaction, followed by a second slower (k_A^s) reaction, when observed in acidic solutions. Following the method of Monsouri and Winterhalter [14], our previous ultraviolet-visible (UV/VIS) spectroscopic study [16] indicated that this biphasic behavior seen in acidic solutions disappeared if the pH of solutions was >8, and became $k_A^f = k_A^s$. This finding leads to certain questions: how does the Hb molecule prompt the range of fast (k_A^f) and slow (k_A^s) components in acidic solutions? How does the molecule provoke $k_A^f = k_A^s$ if the pH of solutions is >8? Does the biphasic autoxidation seen in acidic pH regions reflect a different rate due to the individual Hb chains or the presence of valency hybrid intermediates such as $(\alpha^{2+}\beta^{3+})_2$ and $(\alpha^{3+}\beta^{2+})_2$? Through attempts to locate a site integrating these puzzling problems behind the phenomenon, a pH-sensed molecular device was suggested to exist in the HbO_2 tetramer. Consequently, it was shown that this mechanism produces a tilting of the distal (E7) histidine (His) residue in the β chains at position 63,

thereby preventing the proton-catalyzed displacement of O_2^- by a solvent water molecule [17,18]. The β chains thus acquire pH-dependent delayed autoxidation in the HbO_2 tetramer.

Similar phenomena suggesting participation of an inherent tilting capability of the distal (E7) His residues of the Hb molecule was also very interesting. Following the method of Brunori *et al.* [19], our previous UV/VIS spectroscopic study [20] showed that human HbO_2 obtained from healthy donors tended to degrade to produce hemichrome even at close to physiological temperatures and pH because its occurrence was a function of pH, temperature and the progress of autoxidation of ferrous HbO_2 to the ferric met form. It is known that Heinz bodies are intra-erythrocytic inclusions of hemichrome formed from oxidized or denatured Hb. They have been found and characterized in drug-induced hemolytic anemia, defects in the intra-erythrocytic reducing system (e.g., glucose 6-phosphate dehydrogenase [G-6-PD] deficiency) and in unstable Hb disease [21,22]. Hemichrome is rarely found in erythrocytes *in situ*, so little attention has been paid to hemichrome and formation of Heinz bodies in the context of normal Hb or normal erythrocytes. Nevertheless, we carried out a series of experiments concerning normal Hb and normal erythrocytes based on the hypothesis that formation of Heinz bodies is not only a peculiarity of labile Hb in patients, but is also an innate characteristic of physiologically normal Hb molecules [23,24]. As a consequence, it was shown that the inherent tilting capability of the distal (E7) His residue is closely related to the molecular instability (degradation) of Hb, and that this instability can trigger degradation of the molecule to hemichrome, and subsequent clustering of Heinz bodies within the erythrocyte.

In the studies mentioned above [23,24], Heinz bodies were visualized by exposing blood smears to acetylphenylhydrazine and staining with crystal violet. Changes within the erythrocytes were observed using light microscopy under oil immersion. Prior to the Heinz-body formation (acetylphenylhydrazine) test, blood samples were subjected to mild heating *in vitro* at close to physiological temperatures. The findings indicated that the number of Heinz bodies formed in red cells increased with increasing temperature of the blood sample [23,24]. *In vitro* evaluation of blood fluidity was also conducted under identical conditions using a micro-channel array flow analyzer to give an index of erythrocyte deformability [24]. The equipment included a characteristic V-shaped groove array with micro flow paths (width, 7 μm; length, 30 μm; depth, 4.5 μm) engraved on a single-crystal silicon substrate in an integral circuit. This equipment made it possible to not only observe red cells passing through individual micro-channel arrays by use of an inverted metallographic microscope, but also enabled evaluation of blood fluidity through the groove array in terms of the transit time of the blood sample for a given transit sample volume. The findings indicated that erythrocyte deformability decreased with increasing temperature of the blood sample at >37 °C [24]. In the spleen, Heinz body-containing red cells become trapped while traversing small apertures in the basement membranes separating the cords from the sinusoids (where the spaces are sufficiently small to require extreme deformation of red cells) [25]. Thus, it was suggested that the Hb molecule controls removal of erythrocytes from the blood circulation via triggering degradation of the Hb molecule to hemichrome, and subsequent clustering of Heinz bodies within the erythrocytes depending on the internal and extraneous conditions of the erythrocyte.

Cellular life is relying on rapid and efficient responses to internal and external conditions. The basic molecular events associated with these processes are the structural transitions of the proteins (structural protein allostery) involved [26]. Therefore, the tetrameric human Hb ($\alpha_2\beta_2$; alternatively, a dimer of αβ

protomers) deserves a special position in this field. Hb has two types of αβ interface. One is the α_1–β_1 (and α_2–β_2) and the other is the α_1–β_2 (and α_2–β_1). The latter "sliding" contact is known to be associated with cooperative O_2 binding, and in fact has important roles if the Hb molecule goes from the deoxygenated to oxygenated quaternary structure. However, the role of the former was unclear for a long time. In this regard, important and intriguing observations have been accumulating. Thus, new roles could be attributed for $\alpha_1\beta_1$ (and $\alpha_2\beta_2$). It seems that the α_1–β_1 (and α_2–β_2) interface has dual roles. One is for stabilizing the HbO_2 tetramer against acidic autoxidation and the other is for controlling the fate (removal) of its own erythrocyte from the blood circulation. It seems that the α_1–β_1 (and α_2–β_2) interface produces a conformational constraint in the constructed chains of the Hb molecule via tilting of the distal (E7) His residues. The Hb molecule seems to adequately differentiate between the two types of function (dual roles) responsible for the α_1–β_1 (and α_2–β_2) interface from physiological to cellular. In this overview, we present our findings that led to this conclusion and discuss new roles assigned to the α_1–β_1 (and α_2–β_2) contact.

## 2. Biphasic Autoxidation Curves Observed in Human HbO_2 in Acidic Solutions

In this section, we focus on the biphasic nature of the autoxidation of human HbO_2 seen in acidic solutions. The phenomenon can be described by first-order kinetics containing two rate constants, k_A^f for the initial fast oxidation and k_A^s for the second slower oxidation, respectively, on the basis of our previous report [16]. This issue was the starting point that led us to uncover a new function of the α_1–β_1 (and α_2–β_2) contact existing in the Hb molecule.

HbO_2 was prepared from freshly drawn samples of human blood (total, 50–80 mL) obtained from healthy donors. Samples were centrifuged at $2,400 \times g$ for 10 min to remove supernatant plasma and buffy coats. The erythrocytes obtained were washed five times with ice-cooled 0.9% NaCl solution (saline) by centrifugation and hemolyzed by adding the same volume of ice-cooled distilled water. The hemolysate was then fractionated with ammonium sulfate between 20% saturation and 70% saturation at pH 6.8. After dialysis, this solution was passed through two Sephadex G-50 columns (5×90 cm) equilibrated with 10 mM Tris-HCl (pH 8.6). The effluent Hb fraction was further separated using a diethylaminoethyl (DEAE)-cellulose column (3×15 cm) equilibrated with 10 mM Tris-HCl (pH 8.6) and washed sequentially with stepwise changing of buffer solutions as follows: (i) 60 mM Tris-HCl (pH 8.0); (ii) 100 mM Tris-HCl (pH 7.5); finally (iii) 100 mM NaCl with 100 mM Tris-HCl (pH 8.0). HbO_2 (human adult) was eluted out as the major fraction with 60 mM Tris-HCl (pH 8.0) and used in the experiments after dialyzing against 5 mM Tris-HCl buffer (pH 8.5).

The autoxidation reaction was measured by UV/VIS spectroscopic means in 0.1 M buffer over a wide pH range (5.3–10.5) at 37 °C. Two milliliters of solution containing 0.2 M buffer was placed in a test tube and incubated in a waterbath maintained at 37 ± 0.1 °C using a NESLAB temperature control system (Model RTE-100 or 111 or 210; NESLAB Instruments, Inc., Portsmouth, NH, USA). The reaction was started by adding the same volume of fresh HbO_2 solution (50–125 μM in heme contents). The reaction mixture was then quickly transferred to a spectrophotometric cell (Spectrocell, Type Inject-A-Cell; Funakoshi Co., Tokyo, Japan) with a screwcap stopper. Changes in absorption at 450–650 nm were recorded on the same chart at measured time intervals. Spectra were recorded using an UV/VIS spectrophotometer (JASCO, Model Ubest-50 or V-560 or V-570; Japan

Spectroscopic Co., Tokyo, Japan), equipped with a thermostatically controlled (within ±0.1 °C) cell holder. At the final state of each run, Hb molecules were all completely converted to the ferric met form by addition of potassium ferricyanide. The buffers used were: acetate for pH 4.5–5.5, 2-(*N*-morpholino) ethanesulfonic acid monohydrate (MES) for pH 5.0–6.75, *N*-2-hydroxyethylpiperazine-*N'*-2-ethanesulfonic acid (HEPES) for pH 6.55–8.3, 2-(cyclohexylamino) ethanesulfonic acid for pH 8.2–10.2, and 3-cyclohexylaminopropanesulfonic acid for pH 10.0–10.5.

Figure 1 shows an example of the spectrophotometric changes over time from 450 nm to 650 nm for autoxidation of human HbO_2 when observed in 0.1 M MES buffer (pH 5.3) at 37 °C. In this reaction process, HbO_2 was autoxidized to its ferric met form through the tendency of the bound O_2 to oxidize ferrous heme iron (II) with generation of superoxide anions (O_2^-):

$$\overset{k_A}{Hb(II)O_2 \rightarrow metHb(III) + 4(O_2^-)} \tag{1}$$
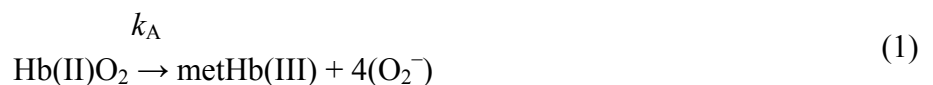
Here k_A represents the observed rate constant of the reaction at a given pH and temperature. The reaction process was followed in each experimental run by the ratio ($[HbO_2]_t/[HbO_2]_0$) of HbO_2 concentration after time t to that at time $t = 0$ that was monitored by the absorbance ratio of $(A_t - A_\infty)/(A_0 - A_\infty)$ at 576 nm (α-peak of HbO_2). The ratio was then plotted against time. Each curve shown in Figure 2 represents the $-\ln([HbO_2]_t/[HbO_2]_0)$ *versus* time plot (first-order plot) for this phenomenon. In acidic solutions (Figure 2(a)), the reaction was biphasic and can be described by first-order kinetics containing two rate constants as follows:

$$d[HbO_2]/dt = P \cdot \exp(-k_A^f \cdot t) + (1 - P) \cdot \exp(-k_A^s \cdot t) \tag{2}$$

Figure 1. Spectral changes over time from 450 nm to 650 nm following human HbO_2 autoxidation, redrawn from Sugawara *et al.* [16]. The changes were monitored in 0.1 M 2-(*N*-morpholino) ethanesulfonic acid monohydrate (MES) buffer (pH 5.3) at 37 °C. Conditions: HbO_2 concentration was 125 μM (in heme contents); the scanning interval was 30 min.
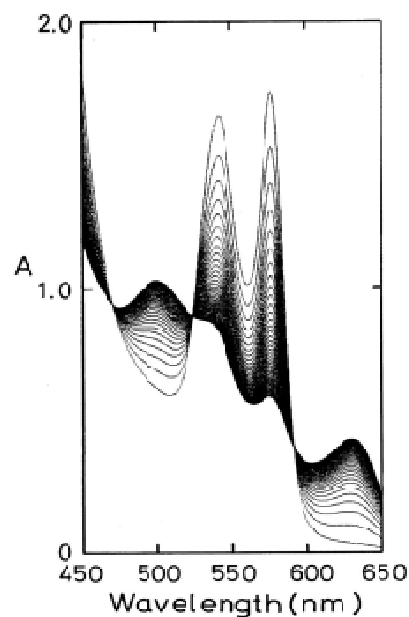
Figure 2. A −ln([HbO$_2$]$_t$/[HbO$_2$]$_0$) *versus* time plot (first-order plot) for human HbO$_2$ autoxidation, redrawn from Sugawara *et al.* [16]. (**a**) Acidic autoxidation seen in acidic-to-neutral pH ranges and (**b**) alkaline autoxidation in alkali solutions. Solid lines represent the least-squares fitting to experimental data in each run. Conditions: HbO$_2$ concentration was 50–125 μM (in heme contents); and the reaction proceeded in 0.1 M buffer at 37 °C.
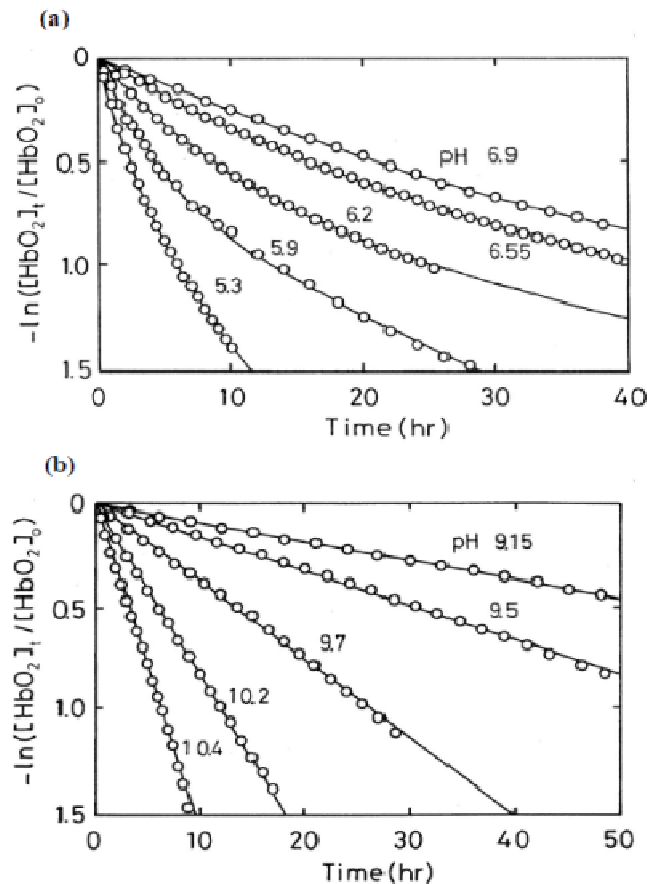
This equation was originally proposed by Monsouri and Winterhalter [14], where $k_A{}^f$ and $k_A{}^s$ represent first-order rate constants for the initial fast oxidation and the second slower oxidation, respectively, and P is the molar fraction of the initial fast component. In Figure 2(a), solid lines represent the best fitting derived by the least-squares method using the equation to each run. However, as shown in Figure 2(b), when the pH of solutions is >8, a plot of −ln([HbO$_2$]$_t$/[HbO$_2$]$_0$) *versus* time showed a single-phase reaction with a single first-order rate constant, although curve fittings could be made using the same equation under conditions of $P = 0.5$ and $k_A{}^f = k_A{}^s$. Thus, it was shown that the biphasic behavior seen in acidic solutions gradually disappeared with increasing pH of solutions and completely disappeared if the pH of solutions was >8.

In this way, the kinetic parameters and molar fraction of the initial fast component (P) for the biphasic nature of human HbO$_2$ autoxidation were established in each run in 0.1 M buffer at 37 °C (Table 1). It was evident that the values of P varied from 0.47 to 0.53. This means that HbO$_2$ was autoxidized with half of the component via the reaction process with the initial fast reaction with $k_A{}^f$ and the other half via the procedure with the second slower rate ($k_A{}^s$). Thus, autoxidation of human HbO$_2$ may be written as follows:

$$k_A^f$$
$$\text{Hb(II)O}_2 \rightarrow 1/2 \text{ metHb(III)} + 4(\text{O}_2^-)$$
$$k_A^s$$
$$\rightarrow 1/2 \text{ metHb(III)}$$

(3)
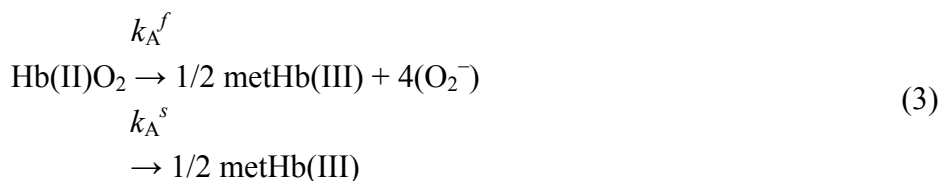
Table 1. Summary of kinetic parameters for the autoxidation of human HbO_2 in 0.1 M buffer obtained by least-squares fitting to the experimental data in each run.

pH	P	k_A^f (h^{-1})	k_A^s (h^{-1})	k_A^s/k_A^f
5.3	0.47	0.438	0.078	0.178
5.9	0.48	0.270	0.030	0.111
6.2	0.48	0.134	0.0154	0.115
6.55	0.49	0.070	0.010	0.142
6.9	0.53	0.0465	0.0073	0.157
9.15	0.50	0.0095	0.0095	1.0
9.5	0.50	0.0184	0.0184	1.0
9.7	0.50	0.0381	0.0381	1.0
10.2	0.50	0.080	0.080	1.0
10.4	0.50	0.157	0.157	1.0

Figure 3. A k_A^s/k_A^f *versus* pH plot for human HbO_2 autoxidation. The solid line stands for the best-suited fitting under the assumption that a single, dissociable group, AH with K_a, can be involved in the reaction. This was achieved with the setting $pK_a = 7.4$.
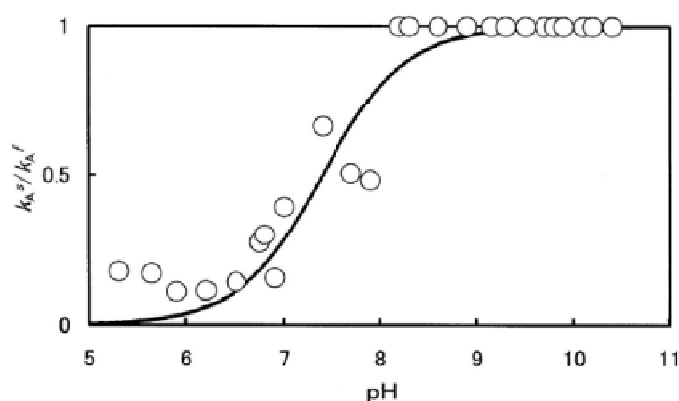
To clarify the processes behind this phenomenon, the obtained values of k_A^s/k_A^f were plotted against the pH of solutions (Figure 3). In Figure 3, the solid line shows that the computed curve obtained by the least-squares method fitted the experimental data over the whole range of pH 5–10.5, where a single dissociable group, AH with K_a, was assumed to be involved in the reaction:

$$K_a$$
$$\text{HbO}_2 \text{ (AH)} \leftrightarrow \text{HbO}_2 \text{ (A}^-)$$

(4)

For neutral amino acids, acid–base equilibrium is usually given by the dissociation constant: $AH \leftrightarrow A^- + H^+$ and thus $K_a = [A^-] \cdot [H^+]/[AH]$. The best fitting was achieved when $pK_a = 7.4$ (at 37 °C). In this regard, Hermans and Rialdi [27,28] reported microcalorimetric ionization data on amino-acid

residues for sperm whale myoglobin (Mb) in which they assigned the His residue with values of $pK_a = 6.62$, the standard Gibbs energy $(\Delta G°) = 37.7 \text{ kJ·mol}^{-1}$, the enthalpy $(\Delta H°) = 29.7 \text{ kJ·mol}^{-1}$, and the entropy $(\Delta S°) = -26.8 \text{ J·mol}^{-1}\cdot\text{K}^{-1}$. It is unwise to identify a dissociation group only by its pK_a value because of the anomalies often found in proteins. Hence, we confirmed that AH must be a His residue assuming that the primary and tertiary structures of α and β subunits are remarkably similar to each other and to Mb. This fact provides information for the existence of a pH-sensed molecular device that can manifest the biphasic autoxidation of the HbO_2 tetramer via participation of a single amino-acid residue with $pK_a = 7.4$ (at 37 °C).

3. Chain Separation and Rate Measurements for the Separated Chains

To not only elucidate the biphasic characteristics of human HbO_2 autoxidation but also to clarify how the Hb molecule can prompt the range of fast $(k_A{}^f)$ and slow $(k_A{}^s)$ components against pH values of the solutions, chain separation of the constituted chains from the parent molecules is essential. In this section, we discuss the results of our study investigating chain separation of α and β chains from the HbO_2 tetramer and their rate measurements.

Isolation of α and β chains from the parent molecules was made using sodium *p*-hydroxymercuribenzoate (*p*-MB) by a one-column method using carboxymethyl (CM)-cellulose and alternatively by a two-column method. The following procedure was for two-column method; details for the one-column method can be found in Sugawara *et al.* [20]. One-hundred milligrams of *p*-MB were dissolved in 2 mL of 0.1 M NaCl and neutralized with 1 M CH_3COOH. This was reacted with 10 mL of HbO_2 solution in 30 mM phosphate buffer, pH 6.0, in the presence of 0.1 M NaCl. To obtain the $\alpha_{p\text{-MB}}$ chains, the mercurated HbO_2 solution was adjusted to pH 8.2 by filtration through a Sephadex G-25 column (25×40 cm) equilibrated with 15 mM HEPES buffer (pH 8.2). The resultant solution was then passed through a DEAE-cellulose column (3×12 cm) equilibrated with the same buffer. Under these chromatographic conditions, the $\alpha_{p\text{-MB}}$ chains were readily eluted out because the unreacted HbO_2 and mercurated β chains were retained on top of the column at this pH. With respect to separation of the $\beta_{p\text{-MB}}$ chains, the pH of the mercurated HbO_2 solution was adjusted to 6.7 using a Sephadex G-25 column (25×40 cm) equilibrated with 10 mM phosphate buffer (pH 6.7) and the solution applied on a CM-cellulose column (3×12 cm) equilibrated with the same buffer. Under these conditions, only the $\beta_{p\text{-MB}}$ chains were eluted completely. Measurement of the autoxidation rate for the isolated chains was identical to the procedure of rate measurements for HbO_2.

Figure 4 shows the pH profiles for the autoxidation rate of the isolated $\alpha_{p\text{-MB}}$ and $\beta_{p\text{-MB}}$ chains. With reference to the rates $(k_A{}^f$ and $k_A{}^s)$ of the parent molecules calculated from biphasic autoxidation curves, the isolated chains were shown to be oxidized much more rapidly to the ferric met-form over the entire pH range (5–10.5) because the reaction followed simple, first-order kinetics as follows:

$$Hb_{sub}(II)O_2 \xrightarrow{k_A{}^{sub}} metHb_{sub}(III) + 4(O_2{}^-) \tag{5}$$
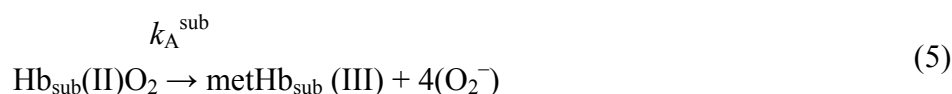
where Hb_{sub} represents each subunit of the Hb molecule. It was also shown that the rate of the initial first component $(k_A{}^f)$ of the parent molecules was found to lie closer to the values of k_A for the isolated $\alpha_{p\text{-MB}}$ and $\beta_{p\text{-MB}}$ chains if the pH of solutions was <6.

Figure 4. Logarithmic values of first-order rate *versus* pH plot for isolated α- and β-chain autoxidation with a reference to the relevant values (k_A^f and k_A^s) of the parent molecules. Conditions: the concentration of isolated α and β chains was 50 μM (in heme contents); the reaction rate was measured in 0.1 M buffer at 37 °C.
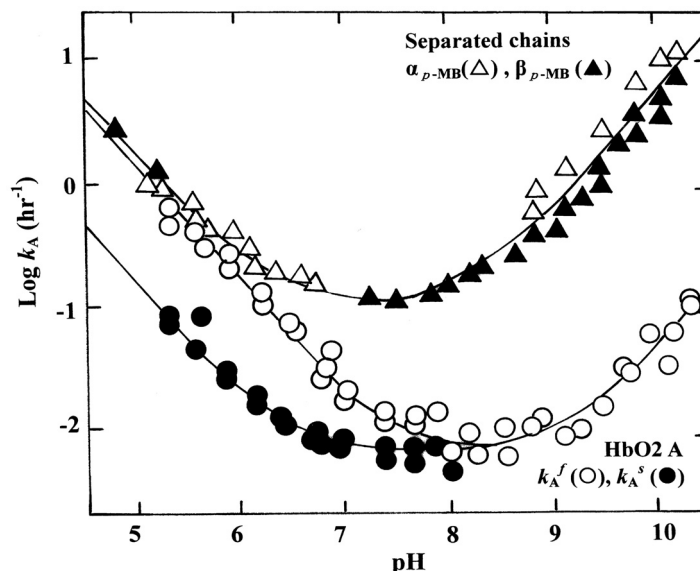
Similar pH profiles were obtained for *p*-MB-removed chains, *i.e.*, the α_{SH} and β_{SH} chains. *p*-MB can be removed from the $\alpha_{p\text{-}MB}$ and $\beta_{p\text{-}MB}$ chains by incubation with 2-mercaptoethanol, as described elsewhere [17]. In separated-chain solutions, the protein is known to exist in equilibrium of α ↔ α₂ or β ↔ β₄, respectively. Under our experimental conditions, the monomeric form (87%) was present in the separated α chain, whereas the tetrameric form (99%) was predominant in the β chain. This estimation was made on the basis of the results by McDonald *et al.* [29].

Thus, it became evident that the isolated α and β chains could be oxidized much more readily over the measured pH range (5–10.5) when compared with the respective rates of the parent molecules as a reference. With respect to the difference in the rate between the isolated individual chains, this seemed to be within reasonable experimental errors in the values of $\alpha_{p\text{-}MB}$ and $\beta_{p\text{-}MB}$ chains, and the α_{SH} and β_{SH} chains.

4. Innate Instability of the Hb Molecule and Its Degradation to Hemichrome

Autoxidation seems to be inseparably related to the instability of the Hb molecule and its degradation to hemichrome. Our previous UV/VIS spectroscopic study [20] showed that human HbO_2 from healthy donors tended to degrade to produce hemichrome even at close to physiological temperatures and pH. In this regard, it has been suggested that the oxidation (autoxidation) process of Hb may be associated with transformation of the oxidized molecule (high-spin Fe^{3+}) into hemichrome, the formation of which can result in the accumulation of soluble and insoluble hemichromes and precipitation [6-11], as mentioned above. Formation of hemichrome is enhanced in separated α and β chains [7,11,19,20,29,30]. In this section, we discuss the innate molecular instability of Hb, which triggers degradation of the molecule to hemichrome. This process is readily detected through UV/VIS spectroscopic observation during the entire process of autoxidation of human HbO_2.

Hemichrome formation could be observed spectroscopically in 0.1 M buffer over a wide range of pH (4.5–10.5) and temperature (35–55 °C). Two milliliters of solution containing 0.2 M buffer were placed in a test tube and incubated in a waterbath maintained at each desired temperature (±0.1 °C) using a NESLAB temperature control system (Model RTE-100 or 111 or 210; NESLAB Instruments, Inc.). The reaction was started by adding the same volume of fresh HbO_2 solution (125–235 μM in heme contents). The reaction mixture was then quickly transferred to a spectrophotometric cell (Spectrocell, Type Inject-A-Cell) with a screwcap stopper. Changes in absorption at 450–650 nm were recorded on the same chart at measured time intervals. Spectra were recorded using a UV/VIS spectrophotometer (JASCO, Model Ubest-50 or V-560 or V-570), equipped with a thermostatically controlled (within ±0.1 °C) cell holder. At the final state of each run, Hb molecules were all completely converted to the ferric met form by the addition of potassium ferricyanide.

Figure 5 shows how autoxidation is inseparably related to the instability of the Hb molecule and its degradation to hemichrome. Figure 5(a) illustrates the spectrophotometric changes over time from 450 nm to 650 nm for hemichrome formation during autoxidation of HbO_2 when HbO_2 was incubated in 0.1 M MES buffer (pH 6.5) at 40 °C. HbO_2 was autoxidized to its ferric met form. However, sudden disruption of the spectra was observed during the late stage of the reaction whereby hemichrome formation could be detected by elevation of the baseline and a shift in isosbestic points caused by precipitation. Hemichrome formation could be readily detected even in HbO_2 at every stage during the course of autoxidation (*i.e.*, during the initial, intermediate, and final stages) while varying the temperature of the solution from 35 °C to 55 °C and the pH from 4.5 to 10.5 (Figure 5(b)). Its occurrence was a function of not only the pH and temperature of the solution, but also of the progress of the autoxidation of HbO_2.

We therefore attempted to categorize the phenomenon into the following four cases in terms of $[HbO_2]_{t = E.P.}/[HbO_2]_0$ (Figure 5(b)):

(1) $t = 0$ or $[HbO_2]_{t = E.P.}/[HbO_2]_0 = 1 \leq t_{E.P.} < [HbO_2]_{t = E.P.}/[HbO_2]_0 = 0.75$;
(2) $[HbO_2]_{t = E.P.}/[HbO_2]_0 = 0.75 \leq t_{E.P} < [HbO_2]_{t = E.P.}/[HbO_2]_0 = 0.25$;
(3) $t_{E.P.} \leq [HbO_2]_{t = E.P.}/[HbO_2]_0 = 0.25$;
(4) no hemichrome formation during the entire process.

E.P. is the observed emergence point of hemichrome formation in each run. $[HbO_2{}_{t = E.P.}/[HbO_2]_0$ is the ratio of HbO_2 concentration after time $t = E.P.$ to that at time $t = 0$ and can be monitored by the absorbance ratio of $(A_t - A_\infty)/(A_0 - A_\infty)$ at 576 nm (α-peak of HbO_2). $[HbO_2]_{t = E.P.}/[HbO_2]_0 = 0.5$ represents equal mixtures of HbO_2 and metHb, *i.e.*, the midpoint of the autoxidation reaction. Hence, case (1) means that hemichrome formation was noticeable at the initial stage of autoxidation. Accordingly, case (2) indicates its occurrence at the intermediate stage, and case (3) at the final stage. In Figure 5(b), the symbols used correspond to: ● for case (1), ▲ for case (2), △ for case (3) and ○ for case (4). To determine if the phenomenon was represented by case (3) or case (4), the reaction mixture was converted to metHb by the addition of small amounts of ferricyanide and maintained at the given temperature for 2 days to see if hemichrome precipitation occurred.

Figure 5. Hemichrome formation associated with human HbO$_2$ autoxidation, redrawn from Sugawara *et al.* [20]. (**a**) Spectral changes over time for hemichrome formation associated with human HbO$_2$ autoxidation in which the reaction was monitored in 0.1 M MES buffer (pH 5.0) at 37 °C and scanning interval = 15 min; (**b**) pH-temperature diagram for hemichrome formation of HbO$_2$. ●—hemichrome formation noticeable at the initial stage during the course of autoxidation; ▲—at the intermediate stage; △—at the final stage; ○—autoxidation reaction proceeded with no hemichrome formation during the entire process.


(a)

(b)
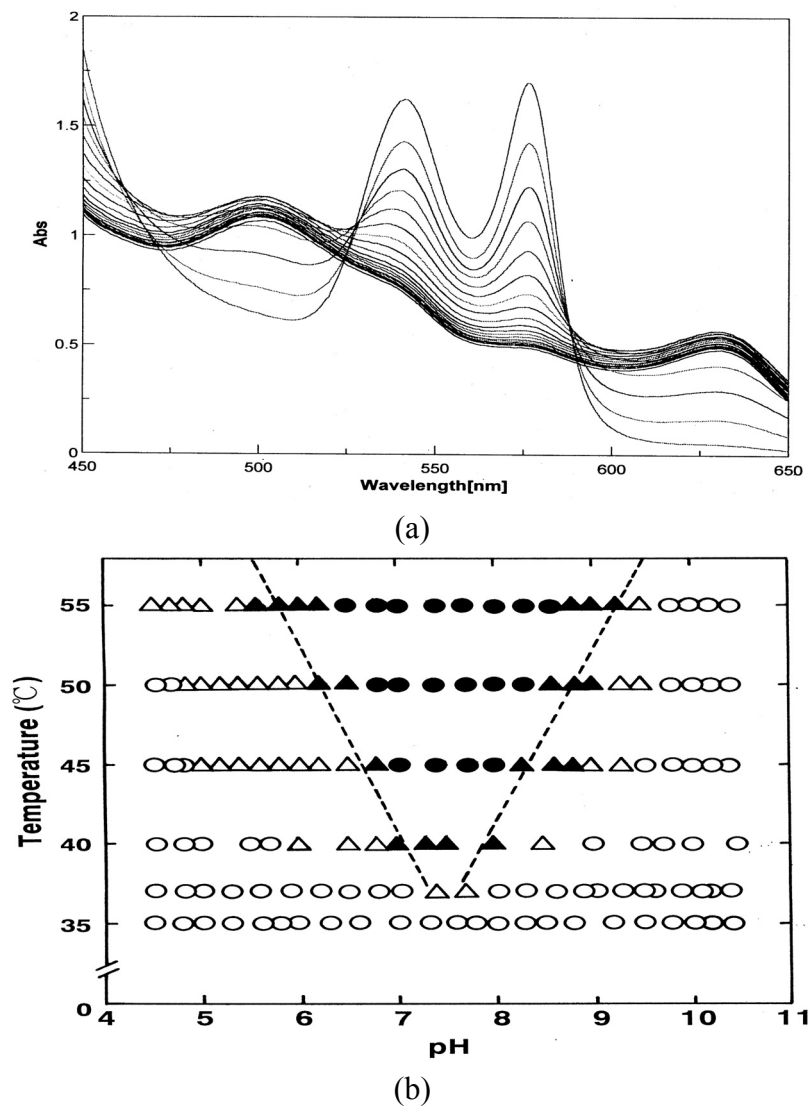
Thus, the findings suggested that HbO$_2$ was highly susceptible to hemichrome formation, even under physiological pH and temperature. The broken lines in Figure 5(b) show that the threshold for this susceptibility in relation to pH and temperature. When compared with the tetrameric parent molecule, the isolated α (α$_{p\text{-MB}}$) and β (β$_{p\text{-MB}}$) chains were found to have much higher susceptibilities to hemichrome formation, and showed individual pH–temperature diagrams (Figure 6). The occurrence of hemichrome can be described as follows:

$$\overset{k_A}{Hb(II)O_2 \rightarrow metHb(III) + 4(O_2^-) \rightarrow hemichrome}$$

(6)
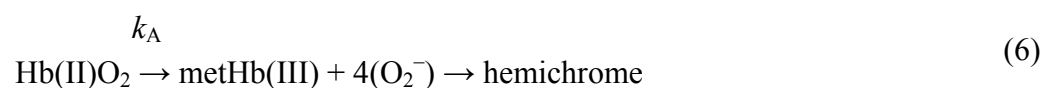
We must be careful when evaluating the data of the isolated chains shown in Figure 4. Because of the instability of Hb molecules and their relationship to hemichrome, the first-order rate constant for the isolated chains was established in each experimental run using only the initial slope of the $-\ln([Hb_{sub}O_2]_t/[Hb_{sub}O_2]_0)$ *versus* time plot. Once hemichrome precipitation arose, one could not get the endpoint spectrum (the ferric met form) of the reaction, whereby Hb molecules in the reaction mixture should be all completely converted to the ferric met form by addition of potassium ferricyanide. Hence, measurement must be confined within the initial range, in which existence of isosbestic points of the spectra that means non-occurrence of hemichrome formation during the entire reaction process was surely guaranteed.

> **Figure 6.** Hemichrome formation for isolated α and β chains, redrawn from Sugawara *et al.* [20]. (**a**) pH-temperature diagrams for hemichrome formation observed in isolated α chains and (**b**) β chains. The symbols are identical to those shown in Figure 5.
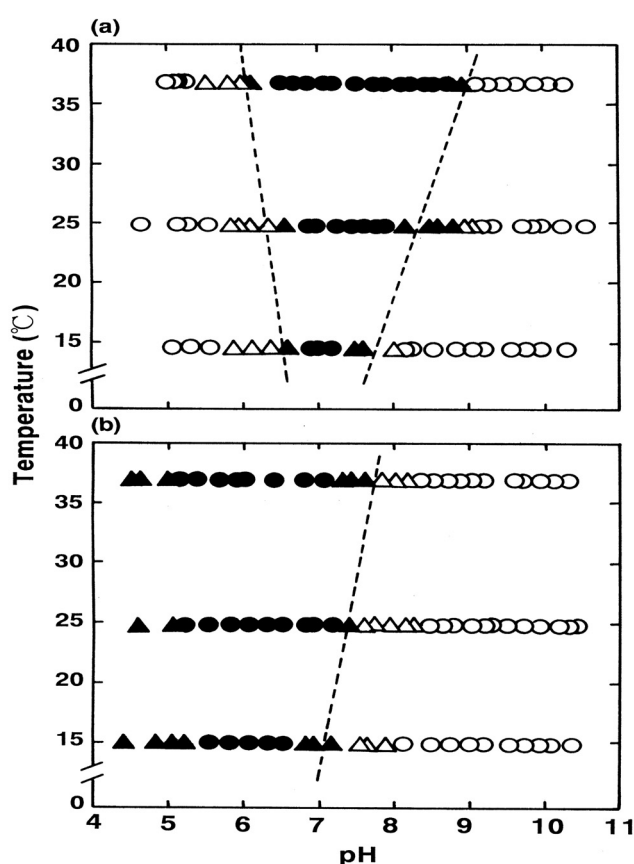
5. UV/VIS Spectrophotometric, Isoelectric-Focusing Electrophoretic and Polyacrylamide Gel Electrophoretic Studies for the Autoxidation of Human HbO₂

In this section, we review our findings resulting from UV/VIS spectrophotometric, isoelectric-focusing electrophoretic and polyacrylamide gel electrophoretic measurements for autoxidation of human HbO_2. It has been demonstrated that the reaction process should be reflected by a different oxidation rate due to different Hb chains [14] or the presence of intermediate Hb with valency hybrids such as $(\alpha^{2+}\beta^{3+})_2$ and $(\alpha^{3+}\beta^{2+})_2$ [15,30-36]. As soon as chain separation was achieved using *p*-MB, 7.5% polyacrylamide gel electrophoresis was undertaken for a series of samples to detect the oxidized ratio of the constituted

chains after time t to that at time $t = 0$. Simultaneously, isoelectric-focusing electrophoresis was carried out for analyzing valency hybrid intermediates on an ampholine plate gel.

The experiment was carried out in 0.05 M phosphate buffer (pH 5.0) in the presence of 20% (*v/v*) glycerol at 37 °C after setting the HbO_2 concentration to 1.25 mM (heme content). We employed a nearly tenfold higher HbO_2 concentration than the usual HbO_2 concentration so that the reaction was monitored using a 1-mm photometric cell instead of a conventional 1-cm cell. Glycerol was used as a protein stabilizer to prevent hemichrome formation during the entire time course of the experiment. For these UV/VIS spectrophotometric, isoelectric-focusing electrophoretic and polyacrylamide gel electrophoretic measurements, an appropriate volume of 0.1 M buffer solution was placed in a test tube and incubated in a waterbath maintained at 37 ± 0.1 °C using a NESLAB temperature control system (Model RTE-1111). The reaction was started by adding the same volume of HbO_2 solution preincubated in the same waterbath. The reaction mixture was then divided into two. One portion was quickly transferred to a spectrophotometric cell with a 1-mm path length (monitoring cell) and the other to a conventional cell with a 1-cm path length (sampling cell). Both cells were maintained at 37 ± 0.1 °C in a thermostated cell holder equipped with a UV/VIS spectrophotometer (JASCO, Model V-560). While monitoring spectrophotometric changes over time from 450 nm to 650 nm in the monitoring cell, sample collection was made from the sampling cell at given intervals. These samples were then submitted to valency hybrid analyses as well as a measurement study for the detection of the oxidized ratio of the constituted chains.

Isoelectric-focusing electrophoresis was carried out using a flatbed apparatus (Model-LKB-Multiphor II, Pharmacia, Uppsala, Sweden). By use of sample application pieces, each 20 μL of sample was applied to a precast ampholine plate gel (ampholine PAGplate, pH 5.5–8.5, Pharmacia) and thereafter an electrophoresis was carried out within 2.5 h under cooling conditions at 10 °C with constant current of 50 mA and constant voltage of 1,600 V. The ampholine plate gel was then fixed for 30 min with fixing solution containing 0.14 M sulfosalicylic acid, 0.7 M trichloroacetic acid, and 7 M methanol. After fixation, densitometric scanning was undertaken using an image scanner (Model AE-6905C; ATTO Co., Tokyo, Japan) allied with computer software.

Also, 7.5% polyacrylamide gel electrophoresis was carried out simultaneously to detect the oxidized ratio of the constituted chains just after chain separation using *p*-MB. With respect to chain separation, *p*-MB (100 mg) was dissolved in 2 mL of 0.1 M NaOH in the presence of 0.1 M NaCl and neutralized with 1 M CH_3COOH. Ten microliters of this solution were then mixed with each 100 μL of a series of collected Hb A samples. Chain separation was continued overnight (~16 h) at 4 °C in 30 mM phosphate buffer (pH 6.0) containing 0.1 M NaCl and 20% (*v/v*) glycerol. Thereafter, electrophoresis was then carried out for 6 h on a 7.5% polyacrylamide slab gel in Tris-glycine buffer (pH 8.6) at a constant current of 12 mA and constant voltage of 150 V. The buffer contained 25 mM Tris and 192 mM glycine. Fixation and staining were undertaken in 7.5% acetic acid containing 1% Coomassie blue. Densitometry was identical to that described for the ampholine plate gel.

The α_{SH} and β_{SH} chains were prepared by removal of *p*-MB with 2-mercaptoethanol from the $\alpha_{p\text{-MB}}$ and $\beta_{p\text{-MB}}$ chains. According to our specifications as described elsewhere [17], the mixture with 15 mM 2-mercaptoethanol was applied on a CM-cellulose column for isolation of the α_{SH} chains, whereas it was on a DEAE-cellulose column for the β_{SH} chains. Each column was then washed with buffer solution containing 2-mercaptoethanol. Thereafter the mercaptoethanol was removed by washing the

column with buffer alone. The buffers used were 10 mM piperazine-*N*, *N′*-bis(2-ethanesulfonic acid) (pH 6.5) for the α_{SH} chains and 10 mM HEPES (pH 8.2) for the β_{SH} chains.

Glycerol was unaffected not only with respect to spectrophotometric changes but also with regard to values of $k_A{}^f$ and $k_A{}^s$. Similarly, there were no quantitative differences between the resulting isoelectric-focusing profiles in the presence or absence of glycerol, whereas the presence of glycerol had a good effect in preventing hemichrome formation during the time course of the experiment.
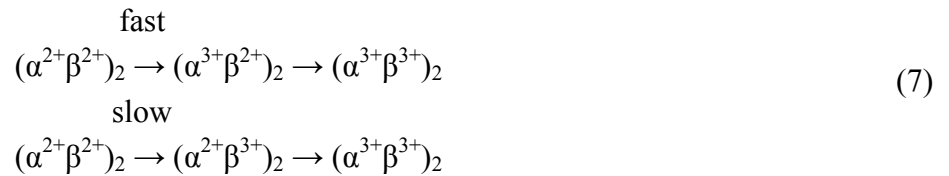
Figure 7 demonstrates UV/VIS spectrophotometric, isoelectric-focusing electrophoretic and polyacrylamide gel electrophoretic measurements in which the reaction proceeded under high HbO_2 concentration (1.25 mM in heme content) in 0.05 M phosphate buffer (pH 5.0) at 37 °C in the presence of 20% (*v/v*) glycerol. Figure 7(a) shows the spectrophotometric changes every 10 min from 450 nm to 650 nm in the monitoring cell. Simultaneously, sample collection was carried out from the sampling cell at 0, 1.2, 2.5, 4.5, 7, 10.5, 16, 25, 42.5, and 76 h. In terms of percentage decrease of HbO_2 concentration in the reaction mixture, the sample picked up at time (*t*) = 0 h corresponded to 100% [HbO_2], and that at: *t* = 1.2 h to 90%; *t* = 2.5 h to 80%; *t* = 4.5 h to 70%; *t* = 7 h to 60%; *t* = 10.5 h to 50%; *t* = 16 h to 40%; *t* = 25 h to 30%; *t* = 42.5 h to 20%; *t* = 76 h to 10%. As mentioned above, these were used for valency hybrid analyses (Figure 7(b)) as well as detection of the oxidized ratio of the constituted chains (Figure 7(c)).

Figure 8 describes the densitometric profiles of the ampholine plate gel shown in Figure 7(b). Four components appeared during the entire reaction process. These had satisfactory-to-good consistency with those reported by Tomoda *et al.* [31-36]. On the basis of the arguments and assignments of Tomoda *et al.*, the first peak must be $(\alpha^{2+}\beta^{2+})_2$, the second can be $(\alpha^{3+}\beta^{2+})_2$, the third can be $(\alpha^{2+}\beta^{3+})_2$, whereas the fourth must be $(\alpha^{3+}\beta^{3+})_2$ as an endpoint. In theory, the following seven species of valency hybrids can be in existence during the entire process: $(\alpha^{2+}\alpha^{2+}\beta^{3+}\beta^{2+})$, $(\alpha^{3+}\alpha^{2+}\beta^{2+}\beta^{2+})$, $(\alpha^{2+}\beta^{3+})_2$, $(\alpha^{3+}\beta^{2+})_2$, $(\alpha^{2+}\alpha^{3+}\beta^{2+}\beta^{3+})$, $(\alpha^{2+}\alpha^{3+}\beta^{3+}\beta^{3+})$ and $(\alpha^{3+}\alpha^{3+}\beta^{3+}\beta^{2+})$. Among these, however, it was evident that only two valency hybrids, *i.e.*, $(\alpha^{3+}\beta^{2+})_2$ and $(\alpha^{2+}\beta^{3+})_2$, emerged in the human HbO_2 autoxidation as demonstrated by Tomoda *et al.* [31,32,35,36]. It was also shown that the appearance (or disappearance) of $(\alpha^{3+}\beta^{2+})_2$ (the second peak) seemed to be preceded by $(\alpha^{2+}\beta^{3+})_2$ (the third peak).

Figure 9 illustrates the densitometric changes of the 7.5% polyacrylamide slab gel (Figure 7(c)) resulting from oxidized ratio analyses of the constituted chains. In contrast to the ampholine plate gel, the obtained electrophoretic migration profiles were complex. Hence, the initial sample (HbO_2) and partially (50%) oxidized sample just after the chain separation using *p*-MB were applied on a 7.5% polyacrylamide slab gel as well as the isolated chains (α_{SH} and β_{SH}) as an endpoint species. These were completely converted to the ferric met form by addition of potassium ferricyanide and thereafter the chain separation procedure was carried out. The resulting densitometric profiles are shown in Figure 10.

Even under these qualified conditions, the profiles were complex. However, it was shown that two bands reflecting fast mobility could be attributed to the α chain, whereas those with medium mobility seemed to be unreacted Hbs with *p*-MB. Two bands found to have relatively slower mobility could have originated from the β chain. From this point of view, designation was made in Figures 9 and 10 as follows: I and II originated from the α chains, III and IV were attributed to unreacted Hbs with *p*-MB, and V and VI derived from the β chains. We could not ascertain which band corresponded to α_{O_2} and α_{met} or β_{O_2} and β_{met}. However, we made an attempt by plotting the ratios of II/I and VI/V against time (Figure 11). It was obvious that a decrease in II/I (as a reflection of α-chain oxidation)

was much faster than a decrease in VI/V (as a reflection due to β-chain oxidation). On the basis of these findings, the reaction can be written as follows:

$$\begin{array}{c} \text{fast} \\ (\alpha^{2+}\beta^{2+})_2 \rightarrow (\alpha^{3+}\beta^{2+})_2 \rightarrow (\alpha^{3+}\beta^{3+})_2 \\ \text{slow} \\ (\alpha^{2+}\beta^{2+})_2 \rightarrow (\alpha^{2+}\beta^{3+})_2 \rightarrow (\alpha^{3+}\beta^{3+})_2 \end{array} \tag{7}$$

Figure 7. The available data resulting from UV/VIS spectrophotometric, isoelectric-focusing electrophoretic and polyacrylamide gel electrophoretic measurements for autoxidation of human HbO_2. The reaction proceeded in the presence of 20% (*v/v*) glycerol in 0.05 M phosphate buffer (pH 5.0) at 37 °C. (**a**) Spectrophotometric changes from 450 nm to 650 nm with scanning interval = 10 min; (**b**) isoelectric-focusing electrophoretic profiles; and (**c**) polyacrylamide gel electrophoretic profiles.


(a)

(b)

(c)
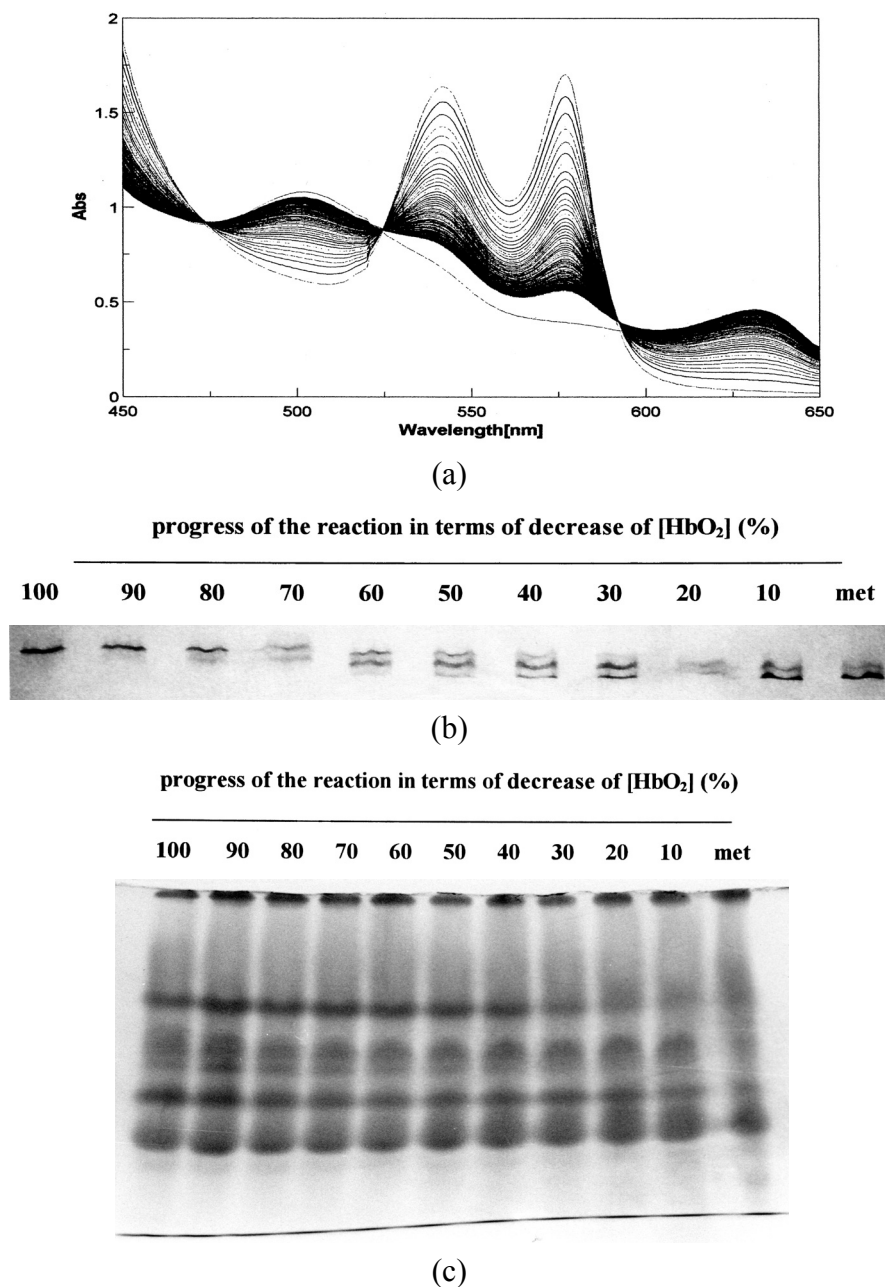
Figure 8. Densitometric profiles resulting from isoelectric-focusing electrophoresis by use of an image scanner. Each curve corresponds to the relevant column shown in Figure 7(b).
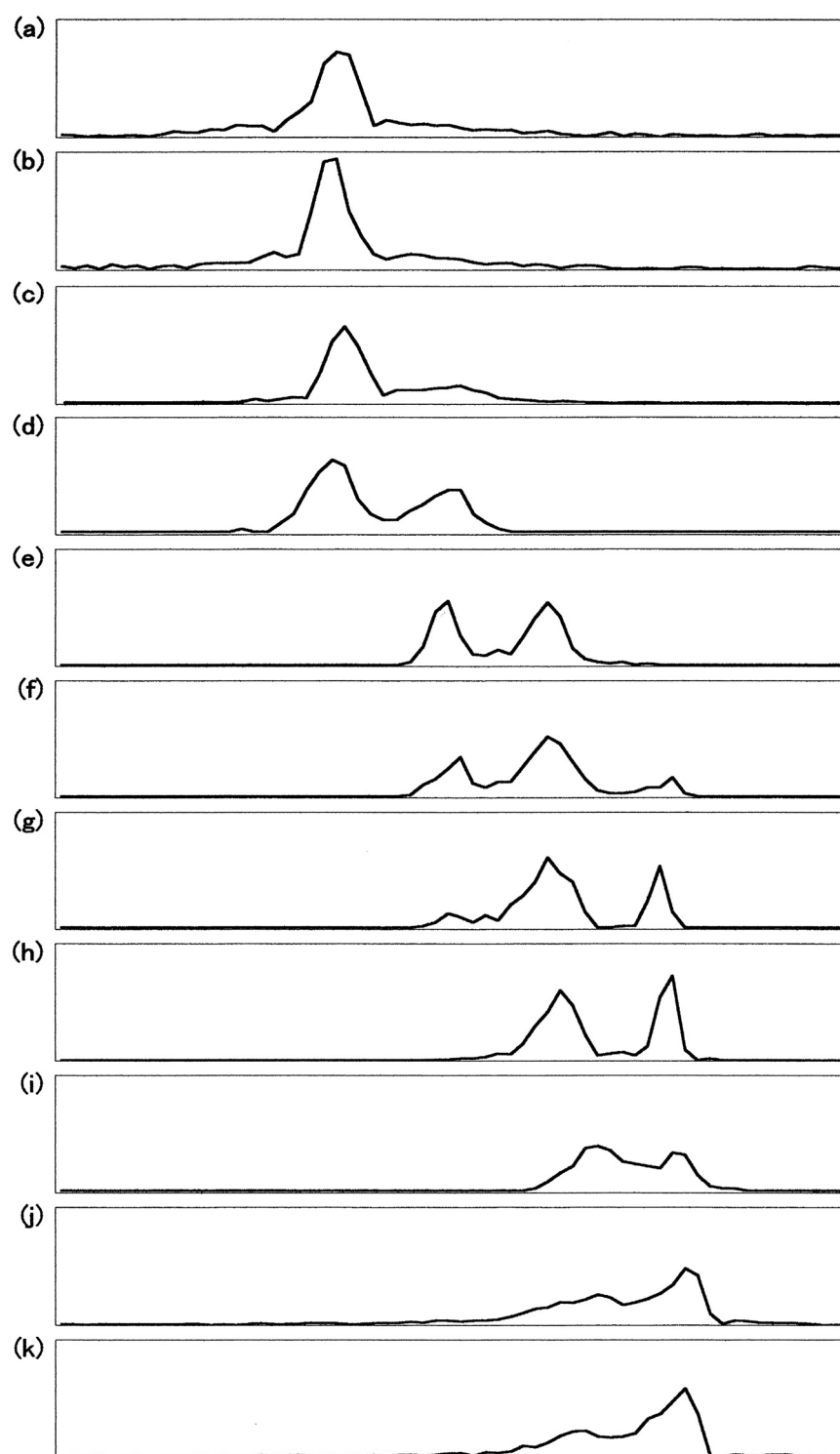
Figure 9. Densitometric profiles resulting from polyacrylamide gel electrophoresis by use of an image scanner. Each curve corresponds to the relevant column shown in Figure 7(c). On the basis of data for qualified samples shown in Figure 10, designation was made as follows: I and II originated from the α chains, III and IV were attributed to unreacted Hbs with *p*-MB, and V and VI derived from the β chains.
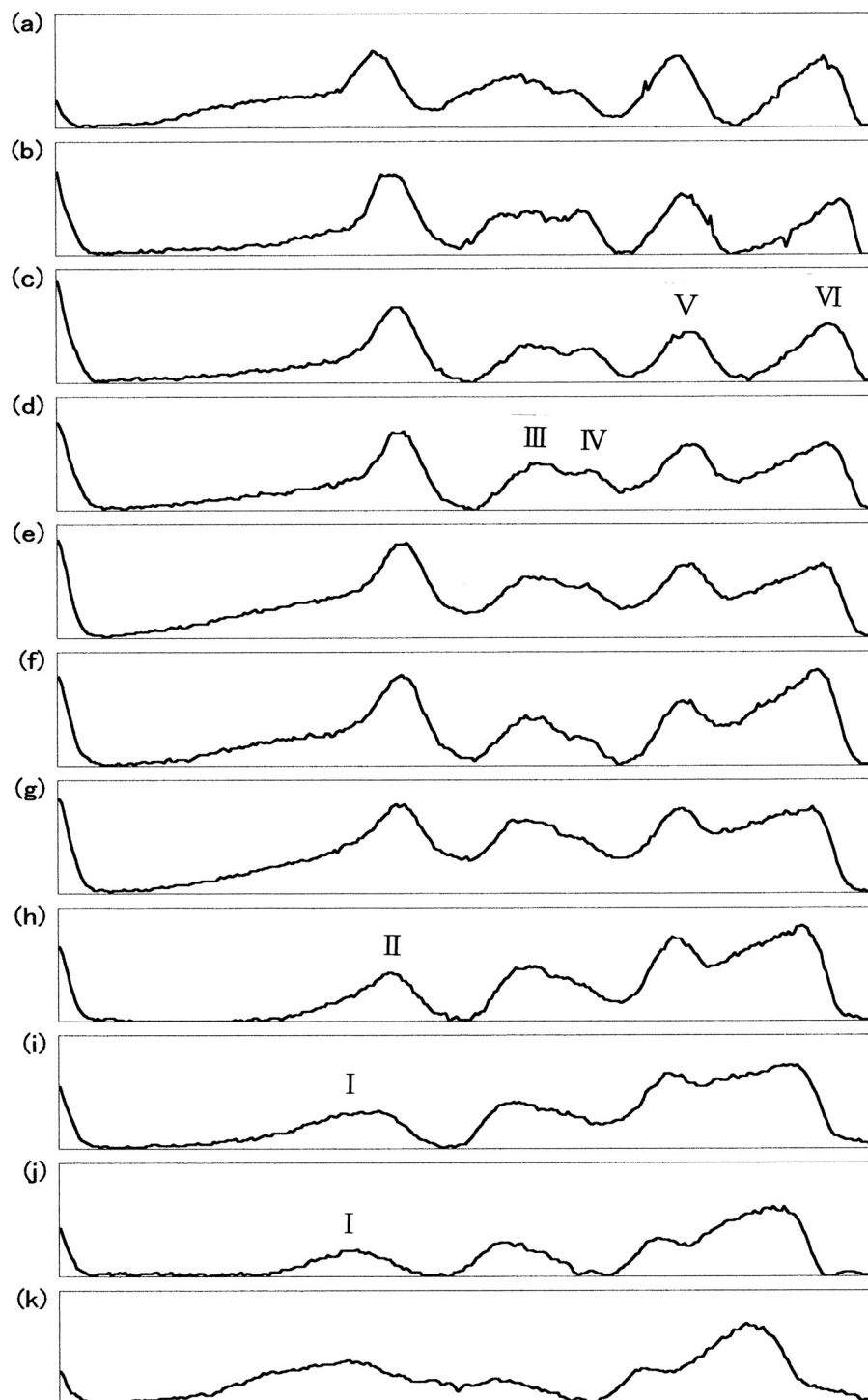
Figure 10. Densitometric profiles of polyacrylamide gel electrophoresis for qualified samples. Densitometric changes correspond to: (**a**) initial HbO_2 sample; (**b**) partially (50%) oxidized sample; (**c**) isolated α_{SH} chain sample as an endpoint product and (**d**) isolated β_{SH} chain sample as the other endpoint species. The isolated chains (α_{SH} and β_{SH}) were completely converted to the ferric met form by addition of potassium ferricyanide. Thereafter, the chain-separation procedure was carried out for the initial HbO_2 sample and partially (50%) oxidized sample.
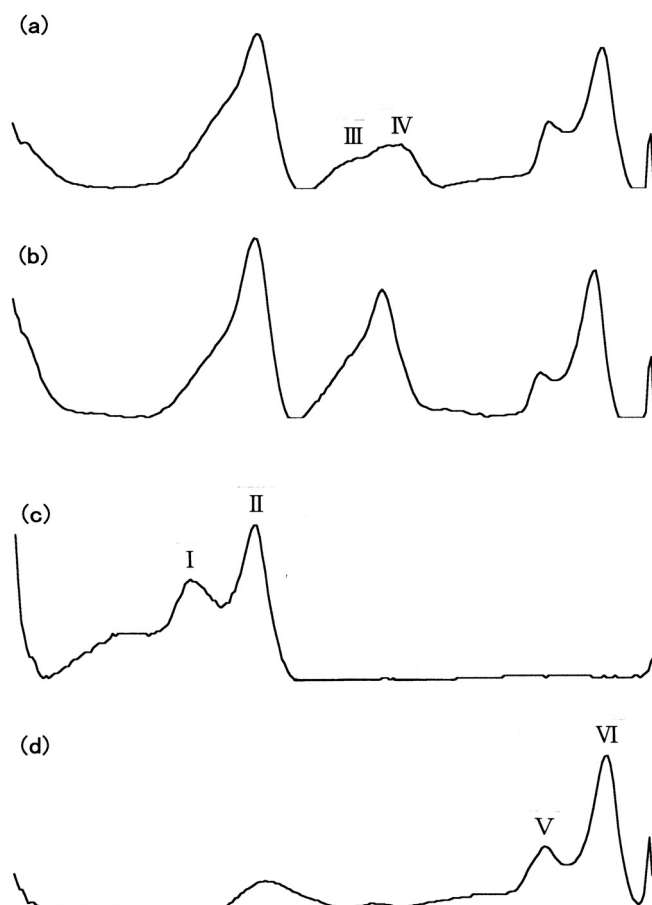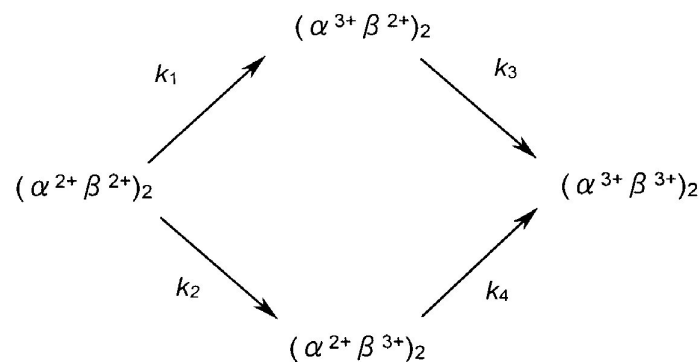

Figure 11. Peak-height ratios of II/I and VI/V *versus* time plots. Peak-height ratios of II/I (○) and VI/V (△) in each column shown in Figure 9 were plotted against time.
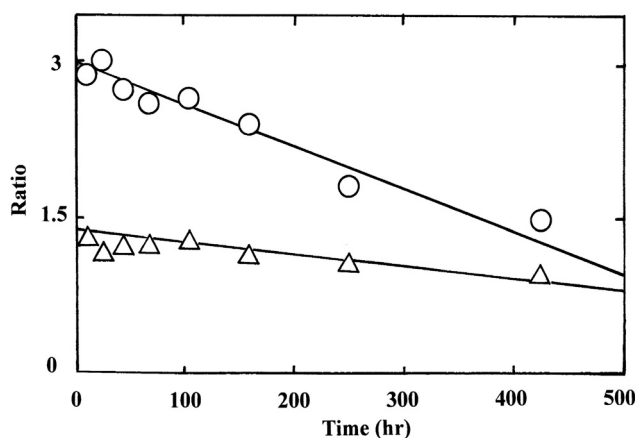
6. Mechanistic Details of Autoxidation of Human HbO₂: Computer Simulations

To shed light on the mechanistic details of human HbO_2 autoxidation, we here propose two tentative models and make a kinetic formulation. Curve fittings were made against the data obtained by UV/VIS spectrophotometric, isoelectric-focusing electrophoretic and polyacrylamide gel electrophoretic measurements. According to our specifications [37] to solve differential equations numerically using the Runge-Kutta method by setting a tentative reaction model, concentration progress curves for species assumed in a given model can be displayed on a personal computer at a given time. The first tentative model can be written as follows:

$$
\begin{array}{ccc}
 & (\alpha^{3+}\beta^{2+})_2 & \\
 {}^{k_1}\nearrow & & \searrow {}^{k_3} \\
(\alpha^{2+}\beta^{2+})_2 & & (\alpha^{3+}\beta^{3+})_2 \\
 {}^{k_2}\searrow & & \nearrow {}^{k_4} \\
 & (\alpha^{2+}\beta^{3+})_2 &
\end{array}
$$

In this scheme, it is assumed that the reaction can proceed via two valency hybrid intermediates, *i.e.*, $(\alpha^{3+}\beta^{2+})_2$ and $(\alpha^{3+}\beta^{2+})_2$. According to the differential equations deduced from the reaction model shown below, we formulated possible pathways leading to the oxidation of Hb to metHb via two valency hybrid intermediates and drew up all the concentration progress curves for the species involved in this reaction.

$$d[(\alpha^{2+}\beta^{2+})_2]/dt = -(k_1 + k_2) \times [(\alpha^{2+}\beta^{2+})_2] \tag{8}$$

$$d[(\alpha^{3+}\beta^{2+})_2]/dt = k_1 \times [(\alpha^{2+}\beta^{2+})_2] - k_3 \times [(\alpha^{3+}\beta^{2+})_2] \tag{9}$$

$$d[(\alpha^{2+}\beta^{3+})_2]/dt = k_2 \times [(\alpha^{2+}\beta^{2+})_2] - k_4 \times [(\alpha^{2+}\beta^{3+})_2] \tag{10}$$

and

$$[(\alpha^{3+}\beta^{3+})_2]_t = [(\alpha^{2+}\beta^{2+})_2]_{t=0} - [(\alpha^{2+}\beta^{2+})_2]_t - [(\alpha^{3+}\beta^{2+})_2]_t - [(\alpha^{2+}\beta^{3+})_2]_t \tag{11}$$

Here the total concentration of Hb ($= [(\alpha^{2+}\beta^{2+})_2]_{t=0}$) is given by the following equation:

$$[(\alpha^{2+}\beta^{2+})_2]_{t=0} = [(\alpha^{2+}\beta^{2+})_2]_t + [(\alpha^{3+}\beta^{2+})_2]_t + [(\alpha^{2+}\beta^{3+})_2]_t + [(\alpha^{3+}\beta^{3+})_2]_t \tag{12}$$

The numerical successive approximation was achieved using the Runge–Kutta method by stepping up one-by-one along with the steps shown in the Appendix.

Figure 12(a) illustrates the best-suited fitting for the consecutive changes of the components attained by isoelectric-focusing electrophoresis while setting $\Delta t = 0.1$ h. In Figure 12(a), the first ($\circ$; $[\alpha^{2+}\beta^{2+}]_2$), second ($\triangle$; $[\alpha^{3+}\beta^{2+}]_2$), third ($\blacktriangle$; $[\alpha^{2+}\beta^{3+}]_2$) and fourth ($\bullet$; $[\alpha^{3+}\beta^{3+}]_2$) components were plotted against time in terms of peak area calculated from the diagrams shown in Figure 8. Each solid line was achieved by non-linear least-squares fitting when setting the kinetic constants as follows: $k_1 = 0.009$ (h^{-1}), $k_2 = 0.002$ (h^{-1}), $k_3 = 0.005$ (h^{-1}), and $k_4 = 0.00008$ (h^{-1}). The resulting curve fittings

show mutually good consistency for the aspects resulting from the isoelectric-focusing electrophoretic study. However, it was evident that the obtained concentration progress curves derived from this model did not fully explain the aspects of spectrophotometric and polyacrylamide gel electrophoretic profiles. Figure 12(b) shows such an example.

Figure 12. Outcomes achieved by a computer simulation using the consecutive reaction model with k_1, k_2, k_3, and k_4 for human HbO_2 autoxidation. (**a**) Isoelectric-focusing electrophoretic changes of the 1st (○), 2nd (△), 3rd (▲) and 4th peaks (●), respectively; and (**b**) the $-\ln([HbO_2]_t/[HbO_2]_0)$ *versus* time plot (first-order plot). Solid lines represent the curves derived from the Runge–Kutta method while setting the following constants: $k_1 = 0.009$ (h^{-1}), $k_2 = 0.002$ (h^{-1}), $k_3 = 0.005$ (h^{-1}), $k_4 = 0.00008$ (h^{-1}) and $\Delta t = 0.1$ h.
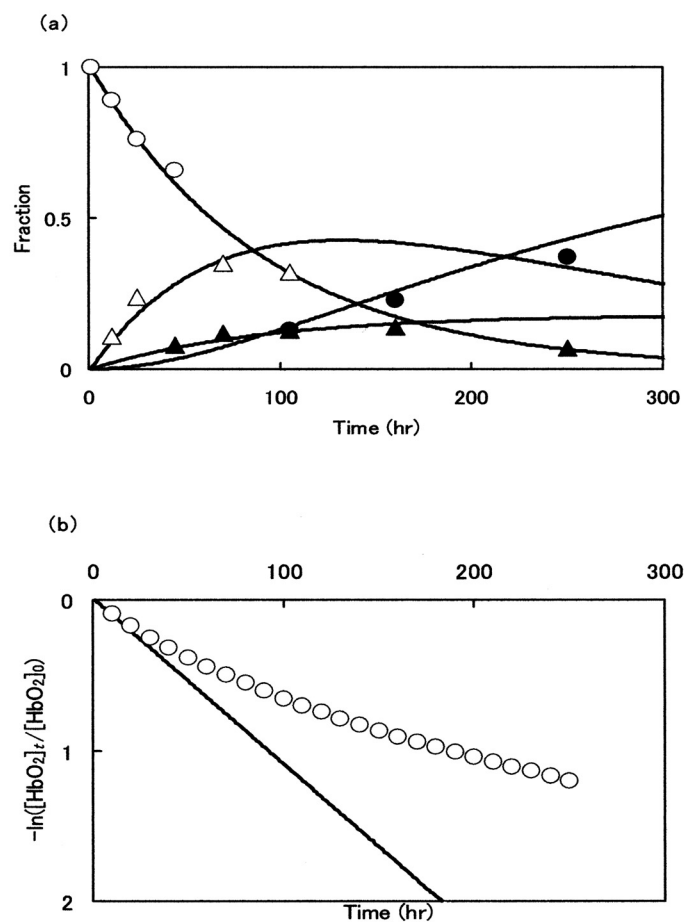
The following second tentative model was thus taken for assessment:
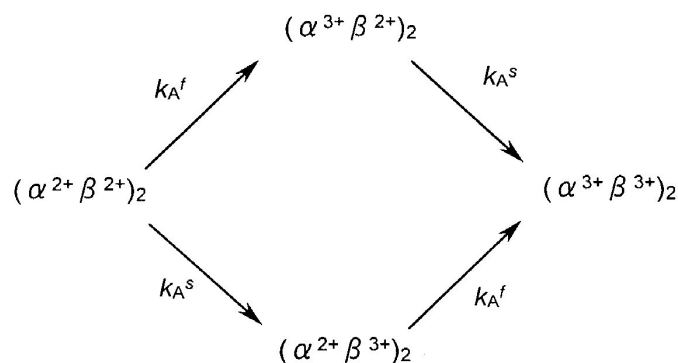
Figure 13. Outcomes achieved by a computer simulation using the consecutive reaction model with k_A^f and k_A^s for human HbO_2 autoxidation. (**a**) The $-\ln([HbO_2]_t/[HbO_2]_0)$ *versus* time plot; (**b**) isoelectric-focusing electrophoretic profiles; and (**c**) polyacrylamide gel electrophoretic profiles. Solid lines represent the curves derived from the Runge–Kutta method with setting of the following constants: $k_A^f = 0.148$ h^{-1}, $k_A^s = 0.0208$ h^{-1} and $\Delta t = 0.1$ h. For (b), the symbols are designated as follows: the 1st ($\circ$), 2nd ($\triangle$), 3rd ($\blacktriangle$) and 4th peaks ($\bullet$), respectively.
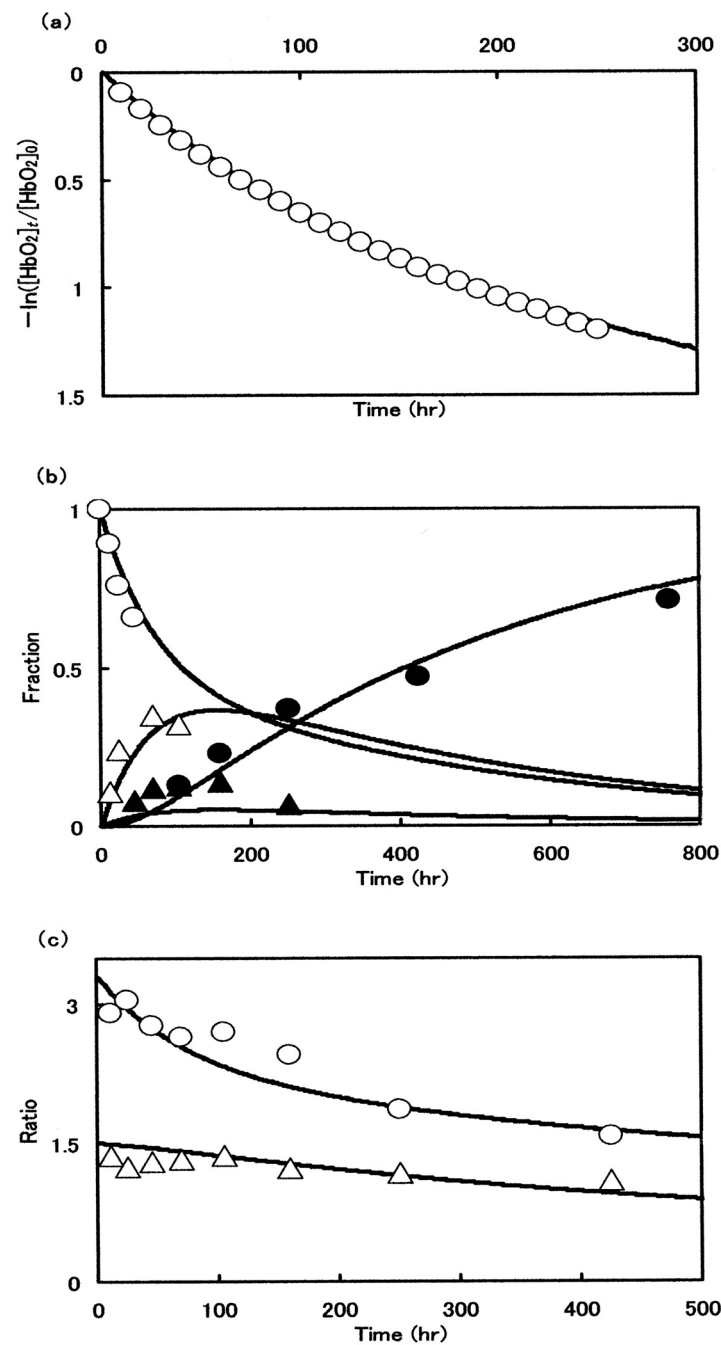
Here k_A^f and k_A^s represent the first-order rate constants calculated from the least-squares fittings against $-\ln([HbO_2]_t/[HbO_2]_0)$ *versus* time plot that was monitored in 0.05 M phosphate buffer (pH 5.0) at 37 °C in the presence of 20% (*v/v*) glycerol (Figure 7(a)). By these least-squares fittings, the following kinetic constants and molar fraction of the initial fast component (*P*) were established:

$k_A{}^f = 0.148$ h^{-1} ($t_{1/2} = 4.7$ h), $k_A{}^s = 0.0208$ h^{-1} ($t_{1/2} = 1.4$ d), and $P = 0.51$. Thus, by setting the values of $k_A{}^f$ and $k_A{}^s$ at 0.148 h^{-1} and 0.0208 h^{-1}, respectively, and $\Delta t = 0.1$ h, the relevant concentration progress curves were displayed on a personal computer for the possible species assumed in this model. Figure 13 illustrates the outcomes: Figure 13(a) shows aspects of the spectrophotometric changes in terms of the $-\ln([\text{HbO}_2]_t/[\text{HbO}_2]_0)$ *versus* time plot, whereas Figure 13(b,c) describe aspects of the associated isoelectric-focusing electrophoretic profiles (Figure 13(b)) and polyacrylamide gel electrophoretic profiles (Figure 13(c)), respectively. In Figure 13, each computed curve (solid line) showed satisfactory-to-good agreements with the experimental data. These demonstrated that almost all of the reaction aspects could be fully explained by the consecutive changes of the species supposed in this model. Thus, the β chain was seen to carry delayed autoxidation in the tetrameric protein architecture. The rate of the initial rapid phase ($k_A{}^f$) characterized with the HbO$_2$ autoxidation represented the intrinsic α-chain oxidation, whereas the rate of the second slower phase ($k_A{}^s$) reflected the intrinsic β-chain oxidation. These findings led us to conclude that the β chain manifests delayed autoxidation in the human HbO$_2$, which could be much more evident in acidic solutions.

7. Innate Instability of the Hb Molecule, Its Degradation to Hemichrome, and Subsequent Formation of Heinz Bodies in Normal Human Erythrocytes during Mild Heating

In this section, we discuss the results of our previous study investigating the formation of Heinz bodies in normal human erythrocytes [23,24]. Aliquots of freshly drawn venous blood from healthy donors were subjected to mild heating at >37 °C for 30 min to investigate hemichrome formation and subsequent Heinz-body formation in normal human erythrocytes. Heinz bodies were then visualized by exposing blood smears to acetylphenylhydrazine and staining with crystal violet. Changes within the erythrocytes were observed using light microscopy under oil immersion.

Prior to the acetylphenylhydrazine test [38,39], blood samples were subjected to mild heating *in vitro*. A 2-mL sample was placed in a test tube and incubated in a waterbath maintained at each desired temperature (±0.1 °C) above 37 °C for 30 min using a NESLAB temperature control system (Model RTE-100 or 111 or 210 or 221). In each experimental run, we employed a temperature-untreated reference as a control. The blood sample used as a temperature-untreated reference was kept at a low temperature (0–4 °C) for as long as possible after withdrawal from the donor, and never exposed to temperatures above room temperature.

β-Acetylphenylhydrazine and crystal violet (research grade for pathology) were used (Wako Pure Chemical, Co., Osaka, Japan) for the procedure, as described by Bauer [39]. A 0.1-mL aliquot of blood sample was suspended in 2 mL of acetylphenylhydrazine solution, in which 100 mg of acetylphenylhydrazine and 200 mg of glucose in 100 mL of 0.067 M phosphate buffer were dissolved at pH 7.6. Using a "blowout" pipette, the solution was aerated twice or thrice by drawing it up into the pipette and blowing it out, together with a small quantity of air. This mixture was incubated at 37 °C for 2 h. Aeration was repeated halfway through and immediately after the 2-h incubation. A drop (~10 μL) of the resulting mixture was placed on a coverslip, which was then inverted onto a microscope slide containing 30 μL of crystal violet solution. The smear was allowed to stand for 20 min in wet preparation at room temperature and subsequently examined under a light microscope (Nikon Model-FXA; Nikon Co., Tokyo, Japan) equipped with a digital camera (Olympus Model-DP-70;

Olympus Co., Tokyo, Japan). Photomicrographs were taken under oil immersion at 1,000× magnification. Subsequently, the number of Heinz bodies per cell was counted in 100 red cells per view.

Figure 14 shows representative images of Heinz bodies within normal red corpuscles (obtained from a healthy donor) during mild heating to a given temperature with using a temperature-untreated reference as a control. Heinz bodies were observed in each smear. Some of the changes are shown in Figure 15(a); histograms of samples treated at 37 °C and 42 °C are displayed with a temperature-untreated sample as a reference based on the number of Heinz bodies contained in each of 100 red cells per view. These results confirmed that Heinz-body formation increased with increasing temperature of blood samples at >37 °C. Red cells in blood samples exposed to 48 °C were hemolyzed.

Figure 14. Microscopic views of Heinz bodies after mild heating of blood samples obtained from one healthy donor, redrawn from Sugawara *et al.* [23,24]. Using a temperature-untreated sample as a control, aliquots of freshly drawn venous blood were subjected to mild heating at 37 °C, 42 °C and 45 °C for 30 min. Heinz bodies were then visualized by exposure to acetylphenylhydrazine and dyeing with crystal violet. The changes that occurred within erythrocytes were observed by light microscopy under oil immersion.
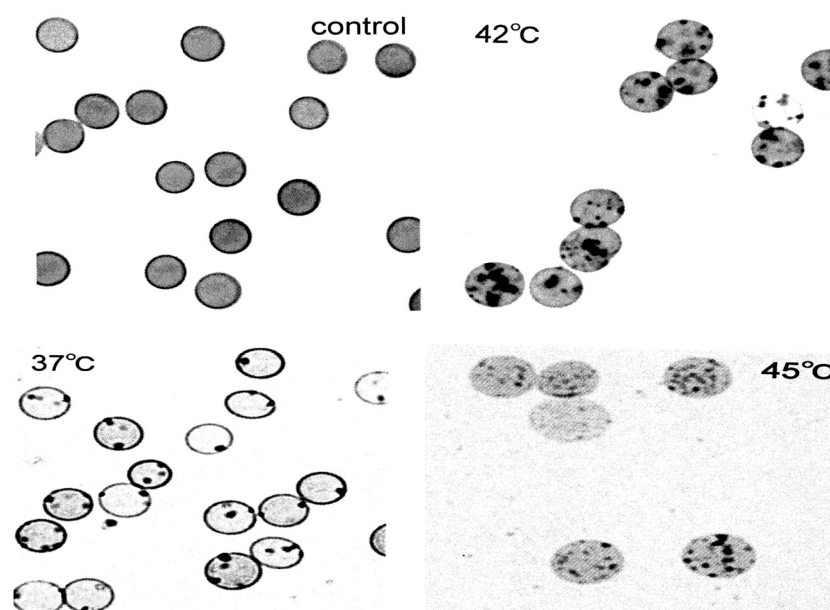

The other histograms shown in Figure 15(b–f) represent the results from another five healthy donors, with a temperature-untreated sample as a reference. Although there was considerable inter-individual variation, temperature-dependent Heinz-body formation was apparent in all preparations. Arithmetic summation was used for all histograms to reduce variability and allow better assessment of temperature-dependent Heinz-body formation. The results of this summation are shown in Figure 16. Solid lines represent the curves derived using the least-squares method using a Gaussian curve. Each computed curve showed satisfactory-to-good agreement with the experimental data over the entire range. The following is a summary of the Gaussian constants resulting from the least-squares fitting: a (peak height) = 101, b (peak width at half of maximum) = 5.0 and c (peak location) = 4.0 for blood samples treated at 42 °C; a = 215, b = 3.5 and c = 1.0 for blood samples treated at 37 °C; and a = 215, b = 3.0 and c = 0.8 for temperature-untreated blood samples.

Figure 15. Histograms representing Heinz bodies detected in blood samples after mild heating at >37 °C, redrawn from Sugawara *et al.* [23,24]. The histograms for 37 °C and 42 °C are displayed using a temperature-untreated sample as a reference. One-hundred red cells were chosen, and the number of Heinz bodies contained in each red cell counted. (**a**) was constructed from the microscopic views shown in Figure 14, whereas (**b–f**) represent the results from another five healthy donors.
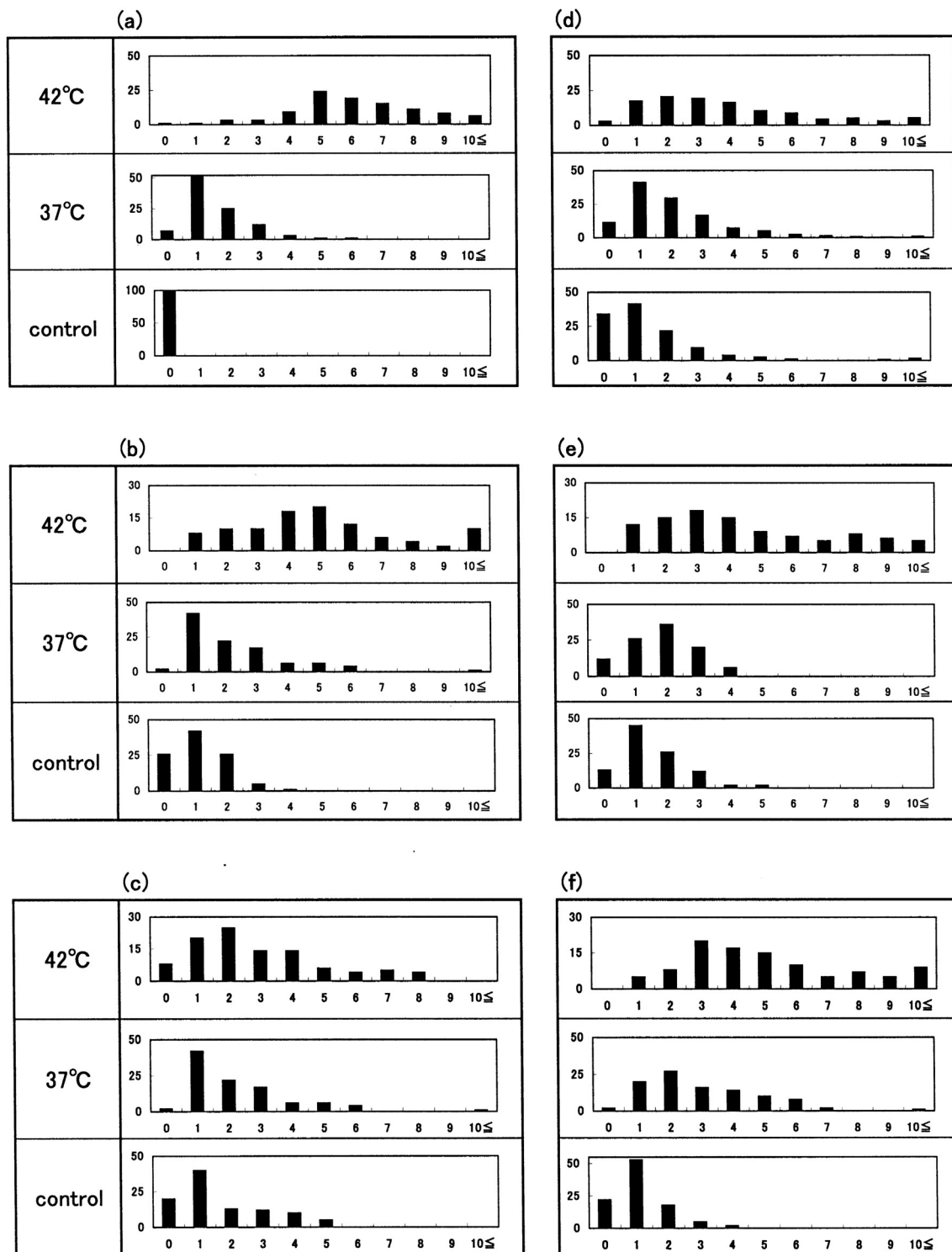
Figure 16. Histograms obtained from the arithmetic summation of all histograms shown in Figure 15, redrawn from Sugawara *et al.* [23,24]. The solid lines show the computed curve obtained by the least-squares method using a Gaussian curve. The resulting Gaussian constants are summarized in the text.
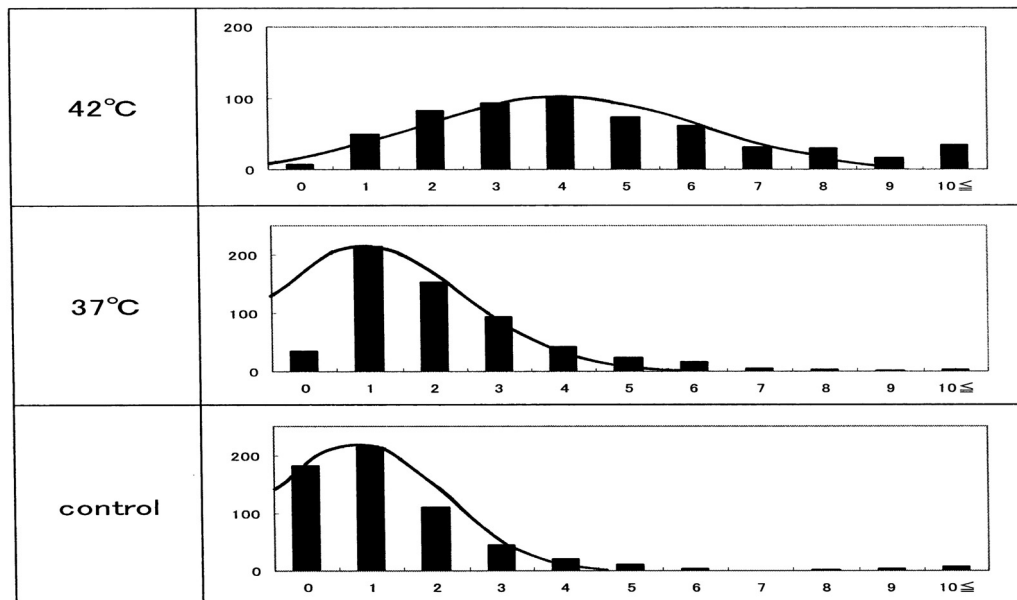
8. *In Vitro* Evaluation of Blood Fluidity during Mild Heating Using a Micro-Channel Array Flow Analyzer to Provide an Index of Erythrocyte Deformability

Kikuchi *et al.* described a tool for measuring the fluidity or rheology of blood [40] in 1992, and this has subsequently been implemented in numerous studies [41-48]. A micro-channel array flow analyzer (MC-FAN) includes a characteristic V-shaped groove array in an integral circuit with 8,736 flow paths (width, 7 μm; length, 30 μm; depth, 4.5 μm) engraved on a 15 × 15 × 0.5-mm single-crystal silicon substrate using an anisotropic etching technique. The array is housed in a cylinder. This equipment makes it possible to not only observe red cells passing through individual micro-channel arrays by use of an inverted metallographic microscope, but also to evaluate blood fluidity through the groove array in terms of the transit time of the blood sample for a given transit sample volume. Flow rate can be determined by timing when the blood sample meniscus crosses graduation marks at 10-μL intervals from 0 μL to 100 μL. The transit sample volume is therefore equivalent to loss of the blood sample within the cylinder. Here we review our *in vitro* findings on blood fluidity during mild heating using a MC-FAN (type-HR300; Hitachi Haramachi Electronics Co., Ibaraki, Japan) [24].

Donors were male or female student volunteers from the Prefectural University of Hiroshima (Hiroshima, Japan) and were aged 18–22 years. All volunteers were aware of the aims and procedures of the study. They gave their written informed consent to participate. The study protocol was approved by the Ethical Review Board of the Prefectural University of Hiroshima. Nine aliquots of samples of freshly drawn venous blood (10 mL in total) were obtained from healthy donors and mixed with one aliquot of 3.2% sodium citrate ($Na_3C_6H_5O_7 \cdot 2H_2O$) or 3.8% sodium citrate ($Na_3C_6H_5O_7 \cdot 5H_2O$). Blood samples were centrifuged at 400 × *g* for 10 min at 0–4 °C to eliminate the possibility of interference with blood fluidity measurements caused by platelet aggregation onto micro-channel flow paths. The

supernatant (platelet-rich plasma (PRP)) was then discarded using a narrow Teflon-lined capillary connected to a waterjet pump. The remainder (PRP-removed blood) was subjected to mild heating prior to application to the MC-FAN. A 2-mL aliquot was placed in a test tube and incubated in a waterbath maintained at each desired temperature ($\pm$0.1 °C) above 37 °C for 30 min using a NESLAB temperature control system (Model RTE-100 or 111 or 210 or 221).

Using a 1-mL disposable syringe and a thin catheter, 200 μL of each temperature-treated blood sample were introduced into a groove array via the cylinder house, which was connected to the inlet hole. The sample was allowed to flow through the cylinder house by applying a pressure difference of 20 cm H_2O. Red cells passing through individual micro-channel arrays were monitored using an inverted metallographic microscope, a video camera, and a video-recorder system. As shown in Figure 17(a,b), microscopic images revealed good erythrocyte deformability in temperature-untreated samples subjected to MC-FAN. However, a marked decline in erythrocyte deformability was observed in blood samples treated at temperatures >37 °C for 30 min. An example is shown in Figure 17(c). Temperature-treated samples also demonstrated increased transit time for low transit sample volumes.

Figure 17. Microscopic details of blood samples passing through individual micro-channel arrays of the micro-channel array flow analyzer (MC-FAN), redrawn from Sugawara *et al.* [24]. (**a**) View of a temperature-untreated sample with a transit time = 12.6 s and transit sample volume = 25 μL. (**b**) Identical temperature-untreated with a transit time = 27.8 s and transit sample volume = 50 μL; (**c**) View of an identical blood sample to that in (a) and (b) but subjected to mild heating at 45 °C for 30 min prior to application to MC-FAN with a transit time = 120.7 s and transit sample volume = 30 μL.

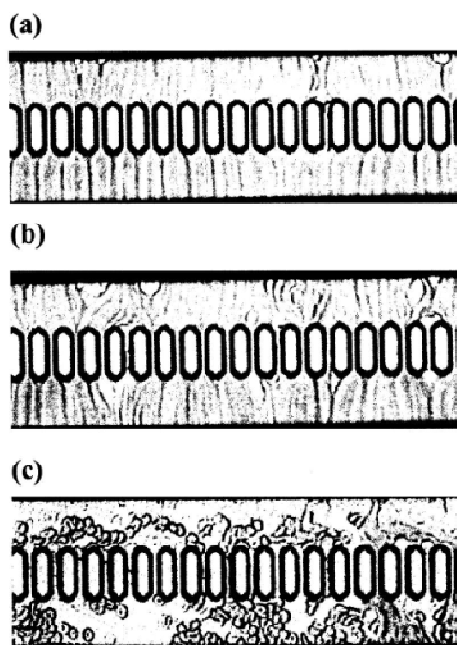

Figure 18 illustrates some examples of blood fluidity of temperature-treated samples measured as transit time *versus* transit sample volume. These graphs show that erythrocyte deformability decreased with increasing temperature at >37 °C, although there was considerable inter-individual variation. Blood was therefore obtained from a further six healthy donors, and temperature-treated samples

compared with a temperature-untreated sample as a reference. The results were similar to those in Figure 18. Both sets of results ($n = 10$) are summarized in Table 2. The temperature-dependent decrease in erythrocyte deformability induced by mild heating was evaluated using the Student's *t*-test on the total sum of the difference in transit times between a given temperature-treated sample and each temperature-untreated reference, with varying transit sample volumes (20, 40 and 60 μL). Significant differences ($p < 0.001$) between treated and control samples were evident for all samples treated at 45 °C with transit sample volumes of 20, 40 and 60 μL, and all samples treated at 42 °C with transit sample volumes of 20, 40 and 60 μL. To adequately show the results of Figure 18, significant differences ($p < 0.001$) of the samples treated at 45 °C (*i.e.*, two-point lines) and 42 °C (*i.e.*, one-point lines) against the control samples (*i.e.*, solid lines) are shown. We therefore concluded that erythrocyte deformability decreased with increasing temperature of blood samples at >37 °C.

Figure 18. Representative examples ($n = 4$) of blood fluidity measured in terms of transit time against transit sample volume, redrawn from Sugawara *et al.* [24]. Solid lines represent the temperature-untreated control; broken lines represent samples treated at 37 °C; one-point lines represent samples treated at 42 °C; two-point lines represent samples treated at 45 °C.
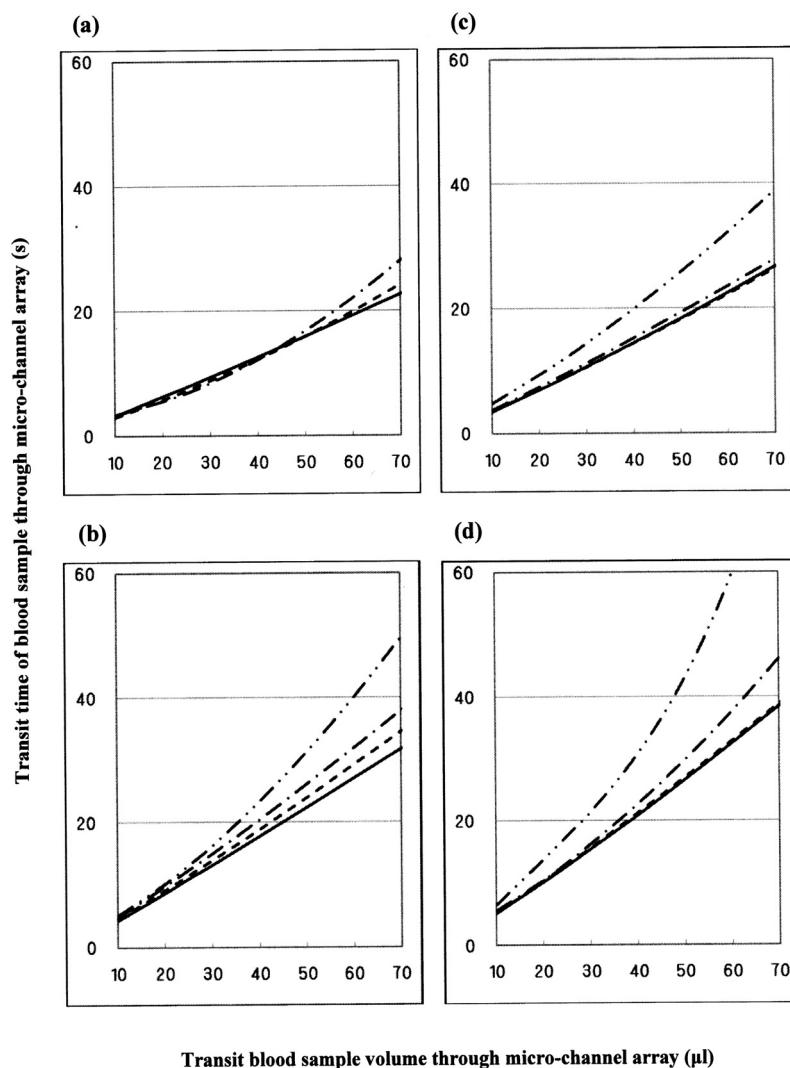
Table 2. Summary of the mean ± standard deviation of transit time of blood samples (s) for a given transit sample volume (µL). Prior to application to MC-FAN, blood samples were subjected to mild heating at 37 °C, 42 °C and 45 °C for 30 min, respectively. The number of subjects was 10. Significant differences ($p < 0.001$) of the temperature-treated samples against the temperature-untreated reference were shown as **.

The mean ± standard deviation of transit time of blood samples (s) for a given transit sample volume (µL)			
	Transit blood sample volume (µL)		
	20 µL	40 µL	60 µL
Temperature-untreated reference	8.0 ± 1.08	16.3 ± 2.24	25.1 ± 3.50
Temperature-treated at 37 °C	7.8 ± 1.35	16.4 ± 2.57	26.4 ± 3.42
Temperature-treated at 42 °C	8.5 ± 1.38 **	18.3 ± 2.94 **	36.3 ± 6.32 **
Temperature-treated at 45 °C	9.3 ± 2.46 **	21.2 ± 5.99 **	41.8 ± 13.23 **

9. Discussion

Cellular life is reliant upon rapid and efficient responses to internal and external conditions. The basic molecular events associated with these processes are the structural transitions of the proteins involved. Therefore, a deeper understanding of the structural bases of protein allostery is of paramount importance to characterize these processes [26]. The human Hb molecule ($\alpha_2\beta_2$; alternatively, a dimer of $\alpha\beta$ protomers), whose α and β chains contain 141 and 146 amino-acid residues, respectively, hold a special position in this field. This is due to the achievements of Perutz, whose pioneering studies led to the identification of two distinct Hb structures, the T (tense) and the R (relaxed) state, which are associated with the deoxygenated and oxygenated form of the protein, respectively [49-51].
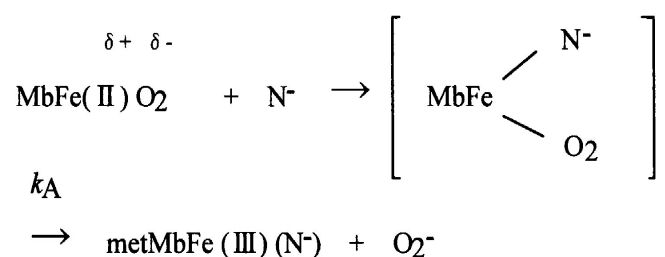
Regarding human HbO_2, a representative set of successive O_2-binding constants is given in terms of $mmHg^{-1}$ as follows: $K_1 = 0.0188$, $K_2 = 0.0566$, $K_3 = 0.407$, $K_4 = 4.28$ in 0.1 M buffer (pH 7.4) containing 0.1 M KCl at 25 °C [52]. In this reaction, by comparing their X-ray crystal structures, major differences have been defined between the deoxygenated and oxygenated forms. These include movement of the iron atom into the heme plane with simultaneous change in the orientation of the proximal (F8) His, rotation of the $\alpha_1\beta_1$ dimer relative to the other $\alpha_2\beta_2$ dimer about an axis P by 12–15°, and a translation of one dimer relative to the other along the P axis by ~1 Å (10^{-1} nm). These changes are accompanied with sequential breaking of "salt bridges" by C-terminal residues [53-57]. When HbO_2 goes from the deoxygenated to the oxygenated quaternary structure, the α_1–β_2 (and α_2–β_1) interface undergoes the principal changes associated with the cooperative oxygen binding, so it is named as the "sliding contact" that involves 19 residues, including mainly helices C and H and the FG corner [55,58].

Conversely, negligible changes are found with respect to the crystal structure examined for the α_1–β_1 (and α_2–β_2) interface that associates 35 residues including B, G, and H helices as well as the GH corner. As mentioned, understanding of subunit interactions between the four Hb chains (and how these explain cooperative O_2 binding) has been the primary focus in Hb research. This has been coupled with a tendency for structural analyses to focus on the changes at the proximal side of the heme and at the α_1–β_2 (and α_2–β_1) interface. This is despite the fact that the configuration of the residues lining the distal side of the heme pocket (where molecular O_2 binds) are also altered by

oxygenation, and are thought to have a role in controlling access of the ligand to the heme pocket [59]. Hence, the possibility of subunit interactions originating from or being transmitted via distal effects has, for the most part, been neglected.

In this overview, we review and summarize the related results and current interpretation of the oxidative behavior of human Hb, emphasizing the correlation between hemichrome emergence and formation of Heinz bodies. Two major subjects discussed and interpreted in terms of the α_1–β_1 (and α_2–β_2) interface are the: (i) pH-dependent delayed autoxidation of β (O_2) subunits when compared with α (O_2) subunits in the tetrameric architecture; (ii) inherent tilting capability of the distal (E7) His residues (*i.e.*, α58His (E7) in the α chain and β63His (E7) in the β chain) to hemichrome formation or Hb degradation.

As with autoxidation, it has been customary to deal with the periphery in Hb research, even though autoxidation is inevitable in nature for all O_2-binding heme proteins. Shikama [60-64] evaluated various mechanisms proposed for autoxidation involving MbO_2 and HbO_2. He clearly demonstrated that the autoxidation reaction does not simply involve the dissociative loss of O_2^- from HbO_2, but is instead caused by the nucleophilic displacement of O_2^- from HbO_2 by a water molecule or a hydroxyl ion that enters the heme pocket from the surrounding solvent. The iron is thus converted to the ferric met form, and the water molecule or hydroxyl ion remains bound to Fe(III) at the sixth coordinate position to form the aqua- or hydroxide-met species. A generalized pathway for this S_N2 mechanism can be written using Mb (MbO_2) as an example:

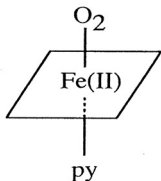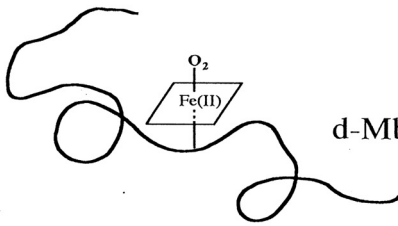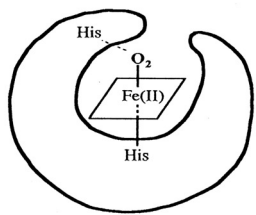$$\overset{\delta+}{M}b\overset{\delta-}{Fe(II)O_2} \ + \ N^- \ \rightarrow \ \left[MbFe \overset{\diagup N^-}{\diagdown O_2} \right]$$

$$\overset{k_A}{\rightarrow} \quad metMbFe(III)(N^-) \ + \ O_2^-$$

Here k_A represents the rate constant of anion-induced autoxidation with nucleophilic anion displacement and N^- can be SCN^-, F^-, OCN^-, N_3^-, or CN^- and, *in vivo*, it can be H_2O or OH^-. Anion-induced autoxidation with nucleophilic anion displacement of O_2 results in an intermediate ferrous heme/anion complex that acts as an electron donor to displace oxygen. Shikama [60,63] also demonstrated that, *in vacua*, oxyheme is inherently stable and unlikely to dissociate O_2^- spontaneously. Because O_2 is a rather poor one-electron acceptor, a considerable thermodynamic barrier exists for such an electron transfer. In aqueous media (*i.e.*, in contrast to *in vacua*), oxyheme is always subject to the nucleophilic attack of an entering water molecule (with or without proton catalysis) and to the attack of an entering hydroxide anion. These can cause irreversible oxidation of oxyheme to met-species with generation of O_2^-. Mb and Hb have therefore evolved with a globin moiety that can protect the Fe(II) O_2 center from the easy access of a water molecule, including its conjugate ions OH^- and H^+.

In an aqueous protein-free system, Kao and Wang [65] reported the oxidation of dipyridine-ferrohemochrome by O_2 using a stopped-flow technique. The main pathway was interpreted to involve one O_2 molecule replacing one of the pyridine molecules in dipyridine-ferrohemochrome to form an oxyheme and then undergoing decomposition to ferrihemochrome and O_2^-. Unfortunately, the rate constant for this oxidation reaction could not be obtained because the concentration term of

pyridine was always involved in its rate equation in a complicated manner. By numerical calculations, however, it follows that oxyheme autoxidation can proceed with a rate constant that is much higher than 1 s^{-1} in 0.1 M buffer, pH 8.5, at 25 °C (Figure 19). If such an oxyheme is placed in a protein matrix, it would be protected against the nucleophilic attack of the solvent water molecule or hydroxyl ion so as to reduce its autoxidation by a factor of $>10^3$. This was the case in our study with denatured MbO_2 in 8 M urea (the details of which can be referred to in Sugawara *et al.* [37]). A globin moiety can act as a "breakwater" in aqueous media even in denatured conditions with 8 M urea. Furthermore, if an oxyheme is embedded in the native Mb architecture, MbO_2 acquires remarkable stability against oxyheme autoxidation by a factor of $\sim10^6$ (Figure 19).

Figure 19. Roles of a globin moiety in Mb or Hb molecules, redrawn from Sugawara *et al.* [37].

With regard to oxyheme stability in human HbO_2, the half-life ($t_{1/2}$) was only 1.5 d in 0.1 M buffer and at physiological pH and temperature [16] even though the content of metHb in normal red cells *in situ* [1,2] has been maintained to be $\leq1\%$ as a consequence of a NADH-dependent reducing system that can reduce the ferric-metHb resulting from autoxidation to deoxy-ferrous Hb [3-5]. However, as compared with the rates of monomeric mammalian Mbs, human HbO_2 seemed to be 2.2–3.6 times more stable against autoxidation (probably due to its tetrameric architecture). Even though the autoxidation rate is a function of pH and temperature, the observed first-order rate constant was 0.0023 h^{-1} ($t_{1/2}$ = 12.6 d) for the human HbO_2 autoxidation under the conditions of 0.1 M buffer at pH 7.2 and 25 °C in our study [10], because this value was calculated from the first rapid phase. Conversely,

the relevant values of the monomeric mammalian Mbs were 0.0082 h^{-1} ($t_{1/2}$ = 3.5 d) for human MbO$_2$, 0.0072 h^{-1} ($t_{1/2}$ = 4.0 d) for bovine MbO$_2$, and 0.0050 h^{-1} ($t_{1/2}$ = 5.8 d) for sperm whale MbO$_2$ under the same conditions of human HbO$_2$.

As mentioned above, the tetrameric human HbO$_2$ showed biphasic autoxidation curve in acidic solutions in terms of the –ln([HbO$_2$]$_t$/[HbO$_2$]$_0$) *versus* time plot; an initial rapid reaction (k_A^f) could be followed with the slower second phase (k_A^s). The difference in the rates between k_A^f and k_A^s decreased with increasing pH value of solutions, and finally disappeared (*i.e.*, $k_A^f = k_A^s$) if the pH of the solutions was >8. A plot for the obtained values of k_A^f/k_A^s *versus* pH indicated that the reaction involves a single dissociation group of amino-acid residue with pK_a = 7.4 (at 37 °C), probably a His residue. In addition, study of rate measurement for the isolated α$_{p\text{-MB}}$ and β$_{p\text{-MB}}$ chains (and α$_{SH}$ and β$_{SH}$ chains) disclosed that once the constituted chains were isolated from the parent molecule, both separated chains could be oxidized much more rapidly to the ferric met-form over the measured pH range (5–10) when compared with the respective rates (k_A^f and k_A^s) of the parent molecules calculated from biphasic autoxidation curves as a reference, and that there could be no practical differences regarding the rate between the isolated individual chains. These findings may mean that the individual chains have acquired considerable resistance to oxyheme autoxidation in their tetrameric protein architecture. It was also suggested that human HbO$_2$ seems to have acquired a pH-sensitive molecular device as a consequence of development of the tetrameric protein architecture. Hence, the molecule shows remarkable stability against oxyheme autoxidation more than in cases of isolated individual chains from the parent molecules and monomeric mammalian Mbs. Moreover, it was evident that only two valency hybrids, *i.e.*, (α^{3+}β^{2+})$_2$ and (α^{2+}β^{3+})$_2$, emerged in the tetrameric HbO$_2$ autoxidation even though, in theory, seven species of valency hybrids can be in existence in theory during the reaction time course: (α^{2+}α^{2+}β^{3+}β^{2+}), (α^{3+}α^{2+}β^{2+}β^{2+}), (α^{2+}β^{3+})$_2$, (α^{3+}β^{2+})$_2$, (α^{2+}α^{3+}β^{2+}β^{3+}), (α^{2+}α^{3+}β^{3+}β^{3+}) and (α^{3+}α^{3+}β^{3+}β^{2+}). Computer simulations on the basis of spectrophotometric, isoelectric-focusing electrophoretic and polyacrylamide gel electrophoretic measurements indicated that k_A^f represents intrinsic α-chain oxidation and k_A^s reflects intrinsic β-chain oxidation. These findings led us to conclude that the β chain manifests delayed autoxidation in human HbO$_2$, which could be much more evident in acidic solutions.

Figure 20. Schematic representation of the role of the α$_1$–β$_1$ (and α$_2$–β$_2$) interface in human HbO$_2$, redrawn from Turuga *et al.* [17]. The α$_1$–β$_1$ (and α$_2$–β$_2$) interface produces in the β chain a tilting of the distal (E7) His residue, thereby preventing the proton-catalyzed displacement of O$_2^-$ by a solvent water molecule.
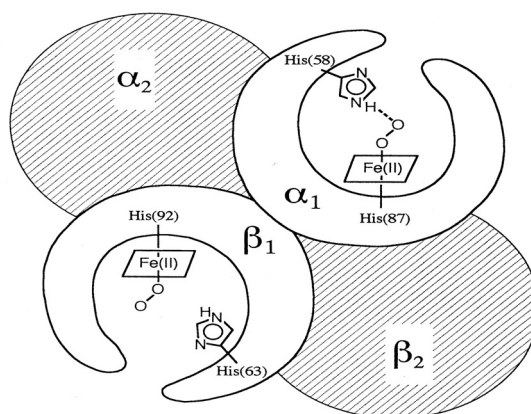
Figure 20 shows our proposal with respect to this issue as reported in 1998 [17] and 2002 [18] in which we suggested a new function to the α_1–β_1 (and α_2–β_2) interface for stabilizing the HbO_2 tetramer against acidic autoxidation. That is, the α_1–β_1 (and α_2–β_2) interface produces a conformational constraint in the β chain whereby the distal (E7) His at position 63 is tilted slightly away from the bound O_2 so as to prevent the proton-catalyzed displacement of O_2^- from the Fe(II)O_2 center by entrance of a water molecule. The β chain thus acquires a remarkably delayed oxidation rate in the HbO_2 tetramer, and this is the origin of the chain heterogeneity seen in acidic solutions of HbO_2 autoxidation.

In fact, the most recent refinement of the crystallographic structure of human HbO_2 (where the O_2 molecule is clearly visible in the high-resolution electron density maps) not only demonstrated that the hydrogen bond made by His E7β (*i.e.*, β63His) is much weaker than that made by His E7α (*i.e.*, α58His), but also substantiated that the geometry of the ligand and distal histidine is slightly different in the two subunits, with the O_2 atom lying 2.7 ± 0.1 Å (10^{-1} nm) from the N^ε atom of the distal histidine in the α subunits, and 3.0 Å away in the β subunits [66]. However, it is an unavoidable fact that negligible changes are found for the α_1–β_1 (and α_2–β_2) interface with respect to examination of the crystal structure.

Similar phenomena suggesting participation of the α_1–β_1 (and α_2–β_2) interface (*i.e.*, participation of the inherent tilting capability of the distal (E7) His residues of the Hb molecule) garnered our interest. As shown in Figures 5 and 6, our UV/VIS spectroscopic study suggested that human HbO_2 was highly susceptible to hemichrome formation even under physiological pH and temperature and, once isolated from the tetrameric parent molecule, the α ($\alpha_{p\text{-MB}}$) and β ($\beta_{p\text{-MB}}$) chains showed much higher susceptibilities to hemichrome when compared with the parent molecule.

Heinz bodies are intra-erythrocytic inclusions of hemichrome formed as a result of Hb oxidation. They have been detected and characterized in drug-induced hemolytic anemia, defects in the intra-erythrocytic reducing system (e.g., G-6-PD deficiency) and in unstable Hb disease [21,22]. Using unstable Hb disease as an example, quite a large number of unstable Hbs have been reported. Regarding the molecular pathogenesis of unstable Hbs, it is known that the instability of labile Hb variants in patients can be attributed to amino-acid substitutions (or deletions), which disrupt and perturb the Hb structure via interference with α-helix formation, disruption of heme binding, or altered α_1–β_1 (and α_2–β_2) or α_1–β_2 (and α_2–β_1) contacts [21]. The consequent changes in circulating red cells in patients with unstable Hb disease include: an inherent tendency towards irreversible denaturation of Hb or globin due to a defect in the amino-acid composition of labile Hb molecules; a continuous tendency toward hemichrome formation; precipitation or aggregation of Hb molecules resulting in buildup of the molecules to form Heinz bodies; and hemolysis.

Exposure of red cells to acetylphenylhydrazine and subsequent staining with crystal violet also revealed a greater abundance of Heinz bodies within G-6-PD-deficient cells compared with that in normal cells [67,68]. In addition, Sear *et al.* [69] and Campwala and Desforges [70] reported that Heinz bodies often appeared in normal-aging red cells, and that this age-related appearance of Heinz bodies was particularly pronounced in splenectomized individuals [71]. According to several authors [72-74], aged or damaged red cells affected by drugs may be "filtered off" by the spleen irrespective of whether or not they contain Heinz bodies in a similar manner to the filtering off of red blood cells in patients with unstable Hb caused by unstable Hb hemolytic anemia.
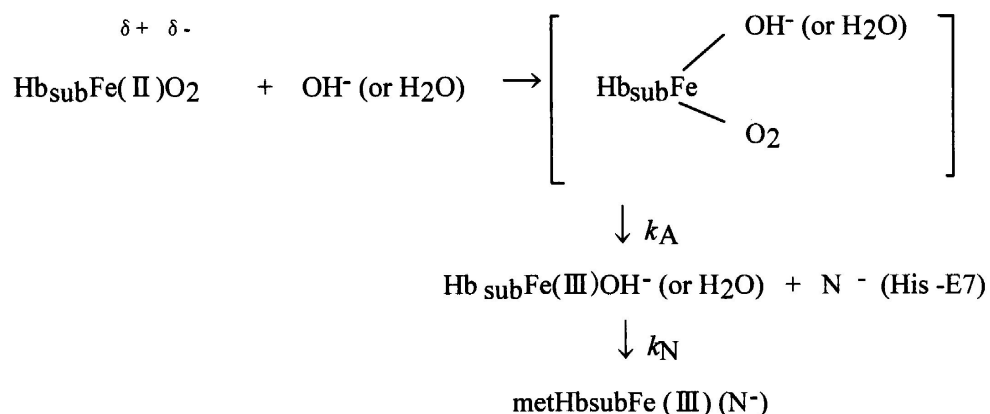
Using freshly drawn venous blood from healthy donors, we found that the number of Heinz bodies formed in red cells increased with increasing temperature when blood samples were subjected to mild heating at >37 °C for 30 min [23,24]. Under identical conditions of mild heating, we measured blood fluidity using a MC-FAN [24] because it involves a characteristic V-shaped groove array with micro flow paths (width, 7 μm; length, 30 μm; depth, 4.5 μm) engraved on a single-crystal silicon substrate in an integral circuit. When red cells passing through individual micro-channel arrays were monitored using an inverted metallographic microscope, images revealed good erythrocyte deformability when temperature-untreated samples were subjected to MC-FAN. Conversely, a marked decline in erythrocyte deformability was observed in blood samples treated at temperatures >37 °C for 30 min. Temperature-treated samples also demonstrated an increased transit time for low transit sample volumes. We therefore concluded that erythrocyte deformability decreased with increasing temperature of blood samples at >37 °C. The combination of our experimental findings and *in situ* observations suggests that instability leading to hemichrome formation is not only a peculiarity of labile Hb variants, but is also an innate characteristic of physiologically normal Hb molecules. In this regard, one must note that monomeric bovine heart MbO_2 did not show a propensity for hemichrome formation over a wide range of pH (4.5–10.5) and temperature from physiological to temperatures just before thermal unfolding [20].

In our experiments, the occurrence of hemichrome can be described as follows:

$$\begin{array}{c} k_A \\ Hb(II)O_2 \rightarrow metHb(III) + 4(O_2^-) \rightarrow hemichrome \end{array} \qquad (13)$$
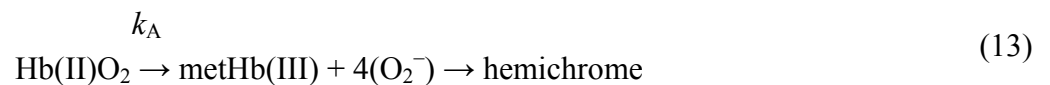
Taking into account the accepted framework of the S_N2 mechanism for autoxidation [59-63] and the accepted framework for hemichrome formation [11] in physiologically conditions, hemichrome can form as follows:

$$\begin{array}{c} \overset{\delta+ \quad \delta-}{Hb_{sub}Fe(II)O_2} \;+\; OH^- \,(or\, H_2O) \;\rightarrow\; \left[Hb_{sub}Fe \overset{\diagup\, OH^-\,(or\,H_2O)}{\diagdown\, O_2} \right] \\[2mm] \downarrow k_A \\[1mm] Hb_{sub}Fe(III)OH^- \,(or\, H_2O) \;+\; N^- \,(His\,\text{-}E7) \\[1mm] \downarrow k_N \\[1mm] metHbsubFe\,(III)\,(N^-) \end{array}$$

In this scheme, Hb_{sub} represents each subunit of the Hb molecule. Nucleophilic displacement of O_2^- by entry of a water molecule or a hydroxyl ion should be the rate-limiting step, and the subsequent conversion of the met form into hemichrome by a heme ligand (N^-) endogenous to the protein must proceed very quickly with the kinetic relationship $k_N \gg k_A$. The most probable candidate for N^- in the HbA molecule is the N^ε-nitrogen of the distal His (E7) (the only amino-acid side chain in the ligand pocket) of each subunit because N^ε-nitrogen is located >4 Å (10^{-1} nm) from the iron in Hb, and is therefore not expected to coordinate in native Hb [11,75].

The content of metHb in normal erythrocytes [1,2] has been reported to be $\leq 1\%$ by a NADH-dependent enzyme system [3-5]. This fact poses the question of how erythrocytes can elicit the range of responses to hemichrome with such a small amount of metHb. We suggest that this can be achieved by intramolecular anion-induced nucleophilic displacement of molecular dioxygen via an intermediate ferrous heme/anion complex (a low-spin hemichrome) [20]. Such a reaction would follow the scheme:

$$\overset{\delta+ \quad \delta-}{Hb_{sub}Fe(II)O_2} + N^-(His\text{-}E7) \rightarrow \left[Hb_{sub}Fe\overset{\nearrow N^-(His\text{-}E7)}{\searrow O_2} \right]$$

$$\overset{k_N}{\rightarrow} metHb_{sub}Fe(III)(N^-) + O_2^-$$
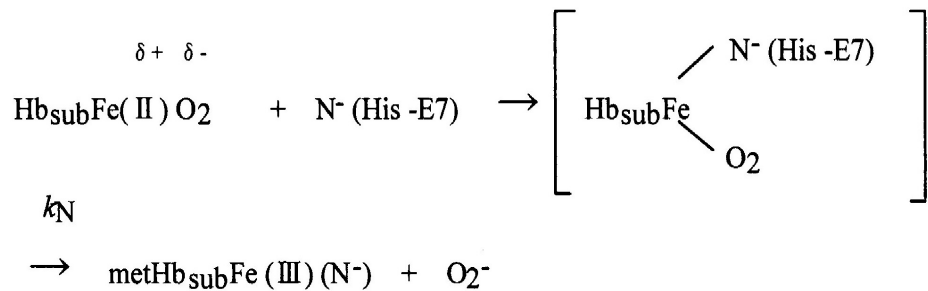
In this reaction, nucleophilic displacement can be caused within the heme pocket by the N^ε-nitrogen of the distal His (E7) instead of nucleophilic incursion of the water molecule or the hydroxyl ion from outside the molecule. As indicated above, hemichrome formation occurs at every stage during the autoxidation reaction of HbO_2 (*i.e.*, at the initial, intermediate, and final stages) as a function of the pH and temperature of the solution. While the reaction proceeds along this scheme, hemichromes may be derived not only from HbO_2 species, but also from deoxyHb and metHb (Figure 21). Vital hemichromes in erythrocytes *in situ* might arise from this intramolecular anion-induced nucleophilic displacement of O_2 via an intermediate ferrous heme/anion complex.

Figure 21. Schematic representation of the role of the α_1–β_1 (and α_2–β_2) interface in human HbO_2 A, redrawn from Sugawara *et al.* [24]. The α_1–β_1 (and α_2–β_2) interface produces a conformational constraint in the constituted chains via tilting of the distal His (E7) residues so as to cause degradation of the Hb molecule to hemichrome, and subsequent Heinz-body clustering within the erythrocyte. In the spleen (which is responsible for the removal of aged and damaged red cells from the blood circulation), Heinz body-containing red cells become trapped and hence undergo hemolysis. By virtue of this endowment, Hb molecules control the fate (removal) of their own erythrocytes from the blood circulation depending on internal and extraneous circumstances, including pH and temperature.
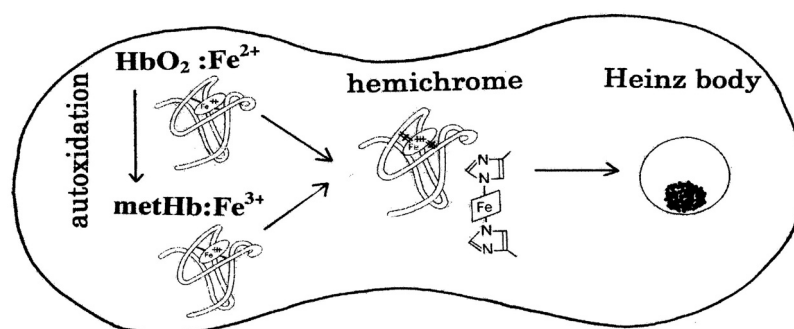
Our electron paramagnetic resonance (EPR) measurement study [17] showed a low-spin spectrum for the resulting oxidation products of isolated β chains with values of $g_1 = 2.77$, $g_2 = 2.27$, and $g_3 = 1.68$, in addition to the usual aquo-met species with g values of 5.86 and 1.99 under a magnetic field of 0–500 mT at 8.0 K in 10 mM maleate buffer (pH 6.2) and in the presence of 50% (*v/v*) glycerol. According to Rifkind *et al.* [11], such low-spin complexes characterized by the highest g values in the range 2.83–2.75 and the lowest g values in the range 1.69–1.63 have been designated as "complex B", indicating the crystal field parameters of the reversible hemichrome (*i.e.*, a water-retained bis-histidine complex). The molar fraction of the hemichrome (complex B) in the oxidized β chains was estimated to be 85% at pH 6.2 because a low-spin species was in equilibrium with a high-spin species corresponding to the usual aquo-met species.

Interestingly, recent crystallographic and EPR spectroscopic studies concerning tetrameric Hbs isolated from the Antarctic fish species *Trematomus bernacchii*, *Trematomus newnesi*, and *Gymnodraco acuticep* show that endogenous coordination at the sixth coordination site of the heme iron could be the bis-histidyl adducts in the ferric state in the solid and solution state [26,76-78]. In Antarctic fish, isolated Hbs are readily oxidized at room temperature to a partial hemichrome state in which only the iron of the β chain is bonded to the distal His. Such bis-histidyl coordination was also discovered in the crystals of horse metHb exposed to acidic pH (where the proximal His [His87(F8)α] and a water molecule are the axial heme ligands) to the hemichrome (bis-histidine) form (in which the proximal His and the distal His [His58(E7)α] are the axial heme ligands) [79]. In the case of horse metHb, the bis-histidyl coordination was seen in α chains, and not in β chains. These crystal structures suggest a different binding state of α and β chains as well as a different pathway to hemichrome.

As described above, the $α_1$–$β_1$ (and $α_2$–$β_2$) interface seemed to have dual faces. One is for stabilizing the HbO_2 tetramer against the acidic autoxidation and the other is for controlling the fate (removal) of its own erythrocyte from the blood circulation. The $α_1$–$β_1$ (and $α_2$–$β_2$) interface produces a conformational constraint in the constructed chains of the Hb molecule via tilting of the distal (E7) His residues, *i.e.*, α58His (E7) in the α chain and β63His (E7) in the β chain. It was also shown that the $α_1$–$β_1$ (and $α_2$–$β_2$) interface appears to have a pH-sensor and a temperature-sensor. By virtue of these endowments, it seemed that Hb molecules can accomplish their roles not only as particularly suitable O_2 carriers between the lungs and tissues but also as equipped "molecular sensors" within the erythrocyte to control the fate (removal) of their own erythrocytes from the blood circulation depending on internal and extraneous circumstances, including pH and temperature (Figure 21).

Regarding the latter issue, normal erythrocytes develop Heinz bodies late in their lifespan. A wide variety of biochemical changes have been reported to accompany the aging of red cells [80]. These include carboxymethylation of proteins, activation of proteases, glycosylation of proteins, loss of membrane area, decline in changes in the ratio of bands 4.1a to 4.1b, increases in oxidized lipids and proteins, changes in the rheology and fragility of cells, changes in the exposure of cell-surface sugars, and gradual accumulation of Ca^{2+} Low [81] demonstrated that band-3 clustering might warrant closer scrutiny as a possible transducer of distress signals from the cytoplasm to the external surface of the cell because it can be caused by hemichrome binding, ATP depletion, malondialdehyde formation, Ca^{2+} accumulation, oxidative crosslinking, or weakening of the skeletal membrane. It is known that hemichromes formed within erythrocytes bind to the cytoplasmic portion of band 3 in the membrane, then rapidly copolymerize with the soluble cytoplasmic domain of membrane band 3, forming an insoluble

copolymer, followed by other changes involved in the pathogenesis of red-cell destruction [82-86]. The dominant role of band-3 clustering suggests that hemichrome formation-induced band-3 clustering could also provide a key to the control of the fate of senescent and damaged red cells in the blood circulation.

Figure 21 also shed light on some clinical aspects of hemoglobinopathies and hemolytic anemia and its associated acute blood loss. Quite a large number of unstable Hbs have been reported [21,22]. Among these, many of the mutants which occur at the α_1–β_2 (and α_2–β_1) interface have altered oxygen affinity, but the bulk of evidence suggests that the α_1–β_1 (and α_2–β_2) interface is much more important in maintaining the molecular stability of Hb than the α_1–β_2 (and α_2–β_1) interface. Hemolytic anemia results from substitutions affecting the α_1–β_1 (and α_2–β_2) interface or the heme pocket. If such mutations occur, the heme iron will be more readily oxidized, and a sequence of events leads to hemichrome formation and subsequent Heinz-body clustering in red cells that causes hemolytic anemia. Typical examples of such variants are shown in Table 3. Surprisingly, almost all of these pathological mutations are found on the β chain, especially in the α_1–β_1 (and α_2–β_2) contact region.

Table 3. Unstable hemoglobin variants, showing sites of amino acid substitutions (or deletions). Each individual row illustrates variant's name, the residue concerned (chain; number; position), and replacement (from → to), respectively.

• E [β26(B8)Glu → Lys]	• Volga [β27(B9)Ala → Asp]
• Genova [β28(B10)Leu → Pro]	• St. Louis [β28(B10)Leu → Gln]
• Tacoma [β30(B12)Arg → Ser]	• Abraham Lincoln [β32(B14)Leu → Pro]
• Castilla [β32(B14)Leu → Arg]	• Philly [β35(C1)Tyr → Phe]
• Rush [β101(G3)Glu → Gln]	• Peterborough [β111(G13)Val → Phe]
• Madrid [β115(G17)Ala → Pro]	• Khartoum [β124(H2)Pro → Arg]
• J. Guantanamo [β128(H6)Ala → Asp]	• Wien [β130(H8)Tyr → Asp]
• Leslie [β131(H9)Gln → deleted]	• Torino [α43(CD1)Phe → Val]
• L. Ferrara [α47(CD5)Asp → Gly]	• Setif [α94(G1)Asp → Tyr]
• St. Lukes [α95(G2)Pro → Arg]	

The situation in patients with G-6-PD deficiency [21,22] can also serve as an example. Red cells are known to be vulnerable to injury by endogenous and exogenous oxidants. Oxidants can be inactivated by reduced glutathione in erythrocytes with normal G-6-PD activity because the pentose phosphate shunt supplies NADPH (which is required for glutathione recycling). In G-6-PD-deficient erythrocytes, however, the reduced glutathione cannot be restored, and the cells sustain irreversible oxidative damage. However, G-6-PD deficiency produces symptoms only if the patient is exposed to an environmental factor that results in increased oxidative stress, including drugs such as antimalarials (e.g., primaquine, pamaquine, dapsone), sulfonamides, nitrofurantoin and phenacetin. The resulting crisis can lead to hemolysis of up to 25–30% of red cells within hours. However, the crisis is self-limited, and only the older population of red blood cells is destroyed. The mechanisms responsible for such an acute hemolytic crisis in patients taking these drugs cannot be explained on the basis of conventional views. However, Figure 21 suggests that this crisis could be triggered by fluctuations in endogenous and exogenous oxidative stress under the fragile pentose phosphate shunt.

Malaria provides another example. This is a protozoal disease transmitted by the bite of female *Anopheles* mosquitoes (*Plasmodium falciparum*, *P. malariae*, *P. vivax*, and *P. ovale*). Blackwater fever syndrome is caused by infection with *P. falciparum*, and is characterized by repeated bouts of chills and fevers, severe intravascular hemolysis and anemia, jaundice, hemoglobinuria (black urine) and splenic enlargement [87-89]. Patients often develop fevers >40 °C. A feature of this disease is that symptoms can be exacerbated in patients with G-6-PD deficiency as a result of taking quinine. In these patients, massive destruction of red cells infected by the parasite occurs, but similar numbers of normal erythrocytes are also ruptured, resulting in characteristic hemoglobinuria. The reason for the massive hemolysis of non-infected red cells is unclear. However, the possibility of a relationship between quinine ingestion and the associated massive hemolysis, as well as the relevance of G-6-PD deficiency, is addressed in Figure 21. Fever >40 °C, endogenous G-6-PD deficiency, and exogenous quinine ingestion represent conditions that induce acute hemolysis, thereby leading to massive blood loss and hemoglobinuria.

10. Conclusions

In the Hb molecule ($\alpha_2\beta_2$), there are two types of $\alpha\beta$ interface (*i.e.*, the $\alpha_1\beta_1$ [and $\alpha_2\beta_2$] and the $\alpha_1\beta_2$ [and $\alpha_2\beta_1$]). In this overview, we made an attempt to assign new functions to the former contact. In contrast to the latter sliding contact that is known to associate with cooperative O_2 binding, and to exhibit principal roles when the Hb molecule goes from its deoxygenated form to oxygenated form, the α_1–β_1 (and α_2–β_2) interface seemed to have dual roles: one for stabilizing the HbO_2 tetramer against acidic autoxidation; the other for controlling the fate (removal) of its own erythrocyte from the blood circulation. The α_1–β_1 interface produces a conformational constraint in the constructed chains of the molecule via tilting of the distal (E7) His residues, *i.e.*, $\alpha58$His (E7) in the α chain and $\beta63$His (E7) in the β chain. In the latter role, it was shown that the α_1–β_1 (and α_2–β_2) interface may exert delicate control of the tilting capability of the distal (E7) His residues to lead to degradation of the Hb molecule to hemichrome, and subsequent Heinz-body clustering within the erythrocyte. In the spleen (which is responsible for the removal of aged and damaged red cells from the blood circulation), rigid intra-erythrocytic hemichrome inclusions (Heinz bodies) are known to act as "sticking points", hence Heinz body-containing red cells become trapped and undergo hemolysis. The Hb molecule seems to differentiate between the two types of function responsible for the α_1–β_1 (and α_2–β_2) interface. By virtue of these endowments, it was demonstrated that Hb molecules accomplish their roles not only as particularly suitable O_2 carriers between the lungs and tissues, but also as equipped molecular sensors within erythrocytes to control the fate of the own erythrocytes from the blood circulation depending on internal and extraneous circumstances, including pH and temperature.

References

1. Paul, W.D.; Kemp, C.R. Methemoglobin: A normal constituent of blood. *Proc. Soc. Exp. Biol. Med*. **1944**, *56*, 55-56.
2. Bodansky, O. Methemoglobinemia and methemoglobin-producing compounds. *Pharmacol. Rev.* **1951**, *3*, 144-196.

3. Scott, E.M.; Duncan, I.W.; Ekstrand, V. The reduced pyridine nucleotide dehydrogenases of human erythrocytes. *J. Biol. Chem.* **1965**, *240*, 481-485.

4. Hultquist, D.E.; Passon, P.G. Catalysis of methemoglobin reduction by erythrocyte cytochrome b_5 and cytochrome b_5 reductase. *Nature* **1971**, *229*, 252-254.

5. Sugita, Y.; Nomura, S.; Yoneyama, Y. Purification of reduced pyridine nucleotide dehydrogenase from human erythrocytes and methemoglobin reduction by the enzyme. *J. Biol. Chem.* **1971**, *246*, 6072-6078.

6. Rachmilewitz, E.A.; Peisach, J.; Bradley, T.B.; Blumberg, W.E. Role of haemichromes in the formation of inclusion bodies in haemoglobin H disease. *Nature* **1969**, *222*, 248-250.

7. Rachmilewitz, E.A.; Peisach, J.; Blumberg, W.E. Studies on the stability of oxyhemoglobin A and its constituent chains and their derivatives. *J. Biol. Chem.* **1971**, *246*, 3356-3366.

8. Rachmilewitz, E.A. Denaturation of the normal and abnormal hemoglobin molecule. *Semin. Hematol.* **1974**, *11*, 441-462.

9. Winterboun, C.C.; Carrell, R.W. Studies of hemoglobin denaturation and Heinz body formation in the unstable hemoglobin. *J. Clin. Invest.* **1974**, *54*, 678-689.

10. Macdonald, V.W. Measuring relative rates of hemoglobin oxidation and denaturation. *Methods Enzymol.* **1994**, *231*, 480-490.

11. Rifkind, J.M.; Abugo, O.; Levy, A.; Heim, J. Detection, formation, and relevance of hemichromes and hemochromes. *Methods Enzymol.* **1994**, *231*, 449-480.

12. Brooks, J. The oxidation of haemoglobin to methaemoglobin by oxygen. *Proc. Roy. Soc. London Ser. B* **1931**, *109*, 35-50.

13. Brooks, J. The oxidation of haemoglobin to methaemoglobin by oxygen II—The relation between the rate of oxidation and the partial pressure of oxygen. *Proc. Roy. Soc. London Ser. B* **1935**, *118*, 560-570.

14. Mansouri, A.; Winterhalter, K.H. Nonequivalence of chains in hemoglobin oxidation. *Biochemistry* **1973**, *12*, 4946-4949.

15. Tomoda, A.; Yoneyama, Y.; Tsuji, A. Changes in intermediate haemoglobins during autoxidation of haemoglobin. *Biochem. J.* **1981**, *195*, 485-492.

16. Sugawara, Y.; Sakoda, M.; Shibata, N.; Sakamoto, H. Autoxidation of human hemoglobin: Kinetic analysis of the pH-profile. *Jpn. J. Phys.* **1993**, *43*, 21-34.

17. Tsuruga, M.; Matsuoka, A.; Hachimori, A.; Sugawara, Y.; Shikama, K. The molecular mechanism of autoxidation for human oxyhemoglobin: Tilting of the distal histidine causes nonequivalent oxidation in the β chain. *J. Biol. Chem*. **1998**, *273*, 8607-8615.

18. Yasuda, J.-P.; Ichikawa T.; Tsuruga, M.; Matuoka, A.; Sugawara, Y.; Shikama, K. The α1β1 contact of human hemoglobin plays a key role in stabilizing the bound dioxygen: Further evidence from the iron valency hybrids. *Eur. J. Biochem.* **2002**, *269*, 202-211.

19. Brunori, M.; Falcioni, G.; Fioretti, E.; Giardina, B.; Rotilio, G. Formation of superoxide in the autoxidation of the isolated α and β chains of human hemoglobin and its involvement in hemichrome precipitation. *Eur. J. Biochem*. **1975**, *53*, 99-104.

20. Sugawara, Y.; Kadono, E.; Suzuki, A.; Yukuta, Y.; Shibasaki, Y.; Nishimura, N.; Kameyama, Y.; Hirota, M.; Ishida, C.; Higuchi, N.; Haramoto, K.; Sakai, Y.; Soda, H. Hemichrome formation observed in human haemoglobin A under various buffer conditions. *Acta. Physiol. Scand.* **2003**, *179*, 49-59.

21. Winslow, R.M.; Anderson, W.F. The Hemoglobinopathies. In *The Metabolic Basis of Inherited Disease*; Stanbury, J.B., Wyngaarden, J.B., Fredricks, D.S., Eds.; McGraw-Hill Book Company: New York, NY, USA, 1978; pp. 1465-1507.

22. Weatherall, D.J.; Clegg, J.B.; Higgs, D.R.; Wood, W.G. The Hemoglobinopathies. In *The Metabolic and Molecular Basis of Inherited Disease*; Scriver, C.R., Beaudet, A.L., William, S.S., Valle, D., Eds.; McGraw-Hill Inc.: New York, NY, USA, 1995; Volume III, pp. 3413-3484.

23. Sugawara, Y.; Abe, Y.; Ohgushi, I.; Ueno, E.; Shimamoto, F. Roles of innate instability characteristic of hemoglobin molecule to hemichrome and subsequent Heinz body formation within normal human erythrocytes. *Res. Rev. Biosci.* **2009**, *3*, 204-215.

24. Sugawara, Y.; Hayashi, Y.; Shigemasa, Y.; Abe, Y.; Ohgushi, I.; Ueno, E.; Shimamoto, F. Molecular biosensing mechanisms in the spleen for the removal of aged and damaged red cells from the blood circulation. *Sensors* **2010**, *3*, 7099-7121.

25. Jacob, H.S. Mechanisms of Heinz body formation and attachment red cell membrane. *Semin. Hematol.* **1970**, *7*, 341-353.

26. Vitagliano, L.; Vergara, A.; Bonomi, G.; Merlino, A.; Verde, C.; Prisco, G.D.; Howes, B.D.; Smulevich, G.; Mazzarella, L. Spectroscopic and crystallographic characterization of a tetrameric hemoglobin oxidation reveals structural features of the functional intermediate relaxed/tense state. *J. Am. Chem. Soc.* **2008**, *130*, 10527-10535.

27. Hermans, J., Jr.; Rialdi, G. Heat of ionization and denaturation of sperm-whale myoglobin determined with a microcalorimeter. *Biochemistry* **1965**, *4*, 1277-1281.

28. Fasman, G.D. Physical and chemical data. In *Handbook of Biochemistry and Molecular Biology*, 3rd ed.; CRC Press: Cleveland, OH, USA, 1976; p. 220.

29. McDonald, M.J.; Turci, S.M.; Mrabet, N.T.; Himelstein, B.P.; Bunn, H.F. The kinetics of assembly of normal and variant human oxyhemoglobin. *J. Biol. Chem.* **1987**, *262*, 5951-5956.

30. Tomoda, A.; Sugimoto, K.; Suhara, M.; Takeshita, M.; Yoneyama, Y. Haemichrome formation from haemoglobin subunits by hydrogen peroxide. *Biochem. J.* **1978**, *171*, 329-335.

31. Tomoda, A.; Takeshita, M.; Yoneyama, Y. Characterization of intermediate hemoglobin produced during methemoglobin reduction by ascorbic acid. *J. Biol. Chem.* **1978**, *253*, 7415-7419.

32. Tomoda, A.; Tsuji, A.; Matsukawa, S.; Takeshita, M.; Yoneyama, Y. Mechanism of methemoglobin reduction by ascorbic acid under anaerobic conditions. *J. Biol. Chem.* **1978**, *253*, 7420-7423.

33. Tomoda, A.; Yubisui, T.; Tsuji, A.; Yoneyama, Y. Kinetic studies on methemoglobin reduction by human red cell NADH cytochrome b_5 reductase. *J. Biol. Chem.* **1979**, *254*, 3119-3123.

34. Tomoda, A.; Yubisui, T.; Tsuji, A.; Yoneyama, Y. Analysis of met-form haemoglobin in human erythrocytes of normal adults and of a patient with hereditary methaemoglobinaemia due to deficiency of NADH-cytochrome b_5 reductase. *Biochem. J.* **1979**, *181*, 505-507.

35. Tomoda, A.; Tsuji, A.; Yoneyama, Y. Mechanism of hemoglobin oxidation by ferricytochrome *c* under aerobic and anaerobic conditions. *J. Biol. Chem.* **1980**, *255*, 7978-7983.

36. Tomoda, A.; Ida, M.; Tsuji, A.; Yoneyama, Y. Mechanism of methemoglobin reduction by human erythrocytes. *Biochem. J.* **1980**, *188*, 535-540.

37. Sugawara, Y.; Matsuoka A.; Kaino, A.; Shikama, K. Roles of globin moiety in the autoxidation reaction of oxymyoglobin: Effect of 8 M urea. *Biophys. J.* **1995**, *69*, 583-592.

38. Demetriou, J.A.; Drewes, P.A.; Gin, J.B. Enzymes. In *Clinical Chemistry*, 2nd ed.; Henry, R.J., Cannon, D.C., Winkelmann, J.W., Eds.; Harper & Row Publishers: New York, NY, USA, 1974; pp. 815-1001.

39. Bauer, J.D. Laboratory investigation of hemoglobin. In *Gradwohl's Clinical Laboratory Methods and Diagnosis*; Sonnenwirtyh, A.C., Jarett, L., Eds.; The C V Mosby Company: ST Louis, MO, USA, 1980; pp. 809-901.

40. Kikuchi, Y.; Sato, K.; Ohki, H.; Kaneko, T. Optically accessible microchannels formed in a single-crystal silicon substrate for studies of blood rheology. *Microvasc. Res.* **1992**, *44*, 226-240.

41. Suganuma, H.; Inakuma, T.; Kikuchi, Y. Amelioratory effect of barley tea drinking on blood fluidity. *J. Nutr. Sci. Vitaminol.* **2002**, *48*, 165-182.

42. Begum, A.N.; Terao, J. Protective effect of quercetin against cigarette tar extract-induced impairment of erythrocyte deformability. *J. Nutri. Biochem.* **2002**, *13*, 265-272.

43. Kamada, H.; Hattori, K.; Hayashi, T.; Suzuki, K. *In vitro* evaluation of blood coagulation activation and microthrombus formation by a microchannel array flow analyzer. *Thromb. Res.* **2004**, *114*, 195-203.

44. Sumino, H.; Nara, M.; Seki, K.; Takahashi, T.; Kanda, T.; Ichikawa, S.; Goto-Onozato, K.; Koya, S.; Murakami, M.; Kurabayashi, M. Effect of antihypertensive therapy on blood rheology in patients with essential hypertension. *J. Int. Med. Res.* **2005**, *33*, 170-177.

45. Watanabe, N.; Kimura, F.; Kojima, F.; Endo, Y.; Fujimoto, K.; Kikuchi, Y. Effect of sterols in dietary fats on whole blood viscosity of stroke-prone spontaneously hypertensive rats (SHRSP). *J. Oleo. Sci.* **2005**, *54*, 1-6.

46. Muranaka, Y.; Kunimoto, F.; Takita, J.; Sumino, H.; Nara, M.; Kuwano, H.; Murakami, M. Impaired blood rheology in critically ill patients in an intensive care unit. *J. Int. Med. Res.* **2006**, *34*, 419-427.

47. Seki, K.; Sumino, H.; Nara, M.; Ishiyama, N.; Nishino, M.; Murakami, M. Relationships between blood rheology and age, body mass index, blood cell count, fibrinogen, and lipids in healthy subjects. *Clin. Hemorheol. Microcirc.* **2006**, *34*, 401-410.

48. Watanabe, N.; Watanabe, Y.; Kumagai, M.; Fujimoto, K. Administration of dietary fish oil capsules in healthy middle-aged Japanese men with a high level of fish consumption. *Int. J. Food Sci. Nutr.* **2009**, *60*, 136-142.

49. Perutz, M.F. Stereochemistry of cooperative effects in haemoglobin. *Nature* **1970**, *228*, 726-739.

50. Perutz, M.F. Nature of haem-haem interaction. *Nature* **1972**, *237*, 495-499.

51. Perutz, M.F; Fermi, G.; Abraham, D.J.; Poyart, C.; Bursaux, E. Hemoglobin as a receptor of drugs and peptides: X-ray studies of the stereochemistry of binding. *J. Am. Chem. Soc.* **1986**, *108*, 1064-1078.

52. Imai, K. Adair fitting to oxygen equilibrium curves of hemoglobin. *Methods Enzymol.* **1994**, *232*, 559-576.

53. Baldwin, J.; Chothia, C. Haemoglobin: The structural changes related to ligand binding and its allosteric mechanism. *J. Mol. Biol.* **1979**, *129*, 175-220.

54. Fermi, G.; Perutz, M.F. Haemoglobin and Myoglobin. In *Atlas of Molecular Structure in Biology*; Phillips, D.C., Richards, F.M., Eds.; Clarendon Press: Oxford, UK, 1981; Volume 2.

55. Dickerson, R.E.; Geis, I. *Hemoglobin: Structure, Function, Evolution and Pathology*; The Benjamin/Cummings Publishing Co., Inc.: Menlo Park, CA, USA, 1983.

56. Perutz, M.F. *Mechanisms of Cooperativity and Allosteric Regulation in Proteins*; Cambridge University Press: Cambridge, UK, 1990.

57. Perutz, M.F.; Wilkinson, A.J.; Paoli, M.; Dodson, G.G. The stereochemical mechanism of the cooperative effects in hemoglobin revisited. *Annu. Rev. Biophys. Biomol. Struct.* **1998**, *27*, 1-34.

58. Borgstahl, G.E.O.; Rogers, P.H.; Arnone, A. The 1.8 Å structure of carbonmonoxy-β4 hemoglobin. *J. Mol. Biol.* **1994**, *236*, 817-830.

59. Levy, A.; Sharma, V.S.; Zhang, L.; Rifkind, J.M. A new mode for heme-heme interaction in hemoglobin associated with distal perturbations. *Biophys. J.* **1992**, *61*, 750-755.

60. Shikama, K. Nature of the FeO_2 bonding in myoglobin: An overview from physical to clinical. *Experientia* **1985**, *41*, 701-706.

61. Shikama, K. Stability properties of dioxygen-iron (II) porphyrins: An overview from simple complexes to myoglobin. *Coord. Chem. Rev.* **1988**, *83*, 73-91.

62. Shikama, K. Autoxidation of oxymyoglobin: A meeting point of the stabilixation and the activation of molecular oxygen. *Biol. Rev.* **1990**, *65*, 517-527.

63. Shikama, K. The molecular mechanism of autoxidation for myoglobin and hemoglobin: A venerable puzzle. *Chem. Rev.* **1998**, *98*, 1357-1373.

64. Shikama, K. Nature of the FeO_2 bonding in myoglobin and hemoglobin: A new molecular paradigm. *Prog. Biophys. Mol. Biol.* **2006**, *91*, 83-162.

65. Kao, O.H.W.; Wang, J.H. Kinetic study of the oxidation of ferrohemochrome by molecular oxygen. *Biochemistry* **1965**, *4*, 342-347.

66. Park, S.-Y.; Yokoyama, T.; Shibayama, N.; Shiro, Y.; Tame, J.R.H. 1.25 Å resolution crystal structure of human haemoglobin in the oxy, deoxy and carbonmonooxy forms. *J. Mol. Biol.* **2006**, *360*, 690-701.

67. Jandel, J.H.; Engle, L.K.; Allen, D.W. Oxidative hemolysis and precipitation of hemoglobin. I. Heinz body anemias as an acceleration of red cell aging. *J. Clin. Invest.* **1960**, *39*, 1818-1836.

68. Peisach, J.; Blumberg, W.E.; Rachmilewitz, E.A. Detection of formation, and relevance of hemichromes and hemochromes. *Biochim. Biophys. Acta* **1975**, *393*, 404-418.

69. Sears, D.A.; Friedman, J.M.; White, D.R. Binding of intracellular protein to the erythrocyte membrane during incubation: The production of Heinz bodies. *J. Lab. Clin. Med.* **1975**, *86*, 722-732.

70. Campwala, H.Q.; Desforges, J.F. Membrane-bound hemichrome in density-separated cohorts of normal (AA) and sickled (SS) cells. *J. Lab. Clin. Med.* **1982**, *99*, 25-28.

71. Selwyn, J.G. Heinz bodies in red cells after splenectomy and after phenacetin administration. *Br. J. Hematol.* **1955**, *1*, 173-183.

72. Weiss, L. The structure of fine splenic arterial vessels in relation to hemoconcentration and red cell destruction. *Am. J. Anat.* **1962**, *111*, 131-179.

73. Weiss, L. The structure of intermediate vascular pathways in the spleen of rabbits. *Am. J. Anat.* **1963**, *113*, 51-59.

74. Wennberg, E.; Weiss, L. Splenic erythroclasia: An electron microscopic study of hemoglobin H disease. *Blood* **1968**, *31*, 778-790.

75. Phillips, S.E.V. Structure of oxymyoglobin. *Nature* **1978**, *273*, 247-248.

76. Vitagliano, L.; Bonomi, G.; Riccio, A.; Prisco, G.D.; Smulevich, G.; Mazzarella, L. The oxidation process of Antarctic fish hemoglobins. *Eur. J. Biochem.* **2004**, *271*, 1651-1659.

77. Vergara, A.; Franzese, M.; Merlino, A.; Vitagliano, L.; Verde C.; Prisco, G.D.; Lee, H.C.; Peisach, J.; Mazzarella, L. Structural characterization of ferric hemoglobins from three Antarctic fish species of the suborder notothenioidei. *Biophys. J.* **2007**, *93*, 2822-2829.

78. Vergara, A.; Franzese, M.; Merlino, A.; Bonomi, G.; Verde, C.; Giordano, D.; Prisco, G.D.; Lee, H.C.; Peisach, J.; Mazzarella, L. Correlation between hemichrome stability and the root effect in tetrameric hemoglobins. *Biophys. J.* **2009**, *97*, 866-874.

79. Robinson, V.L.; Smith, B.B.; Arnone, A. A pH-dependent aquomet-to-hemichrome transition in crystalline horse methemoglobin. *Biochemistry* **2003**, *42*, 10113-10125.

80. Clark, M.R. Senescence of red blood cells: Progress and problems. *Physiol. Rev.* **1988**, *68*, 503-554.

81. Low, P.S. Role of Hemoglobin Denaturation and Band 3 Clustering in Initiating Red Cell Removal. In *Red Blood Cell Aging*; Magnani, M., De Flora, A., Eds.; Plenum Press: New York, NY, USA, 1991; pp. 173-183.

82. Walder, J.A.; Chatterjee, R.; Steck, T.L.; Low, P.S.; Musso, G.F.; Kaiser, E.T.; Rogers, P.H.; Arnone, A. The interaction of hemoglobin with the cytoplasmic domain of band 3 of the human erythrocyte membrane. *J. Biol. Chem.* **1984**, *259*, 10238-10246.

83. Waugh, S.M.; Low, P.S Hemichrome binding to band 3: Nucleation of Heinz bodies on the erythrocyte membrane. *Biochemistry* **1985**, *24*, 34-39.

84. Low, P.S.; Waugh, S.M. The role of hemoglobin denaturation and band 3 clustering in red blood cell aging. *Science* **1985**, *227*, 531-533.

85. Schlueter, K.; Drenckhahn, D. Co-clustering of denatured hemoglobin with band 3: Its role in binding of autoantibodies against band 3 to abnormal and aged erythrocytes. *Proc. Natl. Acad. Sci. USA* **1986**, *83*, 6137-6141.

86. Waugh, S.M.; Walder, J.A.; Low, P.S. Partial characterization of the copolymerization reaction of erythrocyte membrane band 3 with hemichromes. *Biochemistry* **1987**, *26*, 1777-1783.

87. Ende, J.V.D.; Coppena, G.; Verstraeten, T.; Haegenborgh, T.V.; Depraetere, K.; Gompel, A.V.; Enden, E.V.D.; Clerinx, J.; Colebunders, R.; Peetermans, W.E.; *et al*. Recurrence of blackwater fever: triggering relapses by different antimararials. *Trop. Med. Inter. Health.* **1998**, *3*, 632-639.

88. White, J.M. Mararia. In *Manson's Tropical Diseases*; Cook, G.C., Zumura, A.I., Eds.; W.B. Saunders: Philadelphia, PA, USA, 2003; pp. 1205-1295.

89. Hue, N.T.; Charlieu, J.P.; Chau, T.T.H.; Day, N.; Farra, J.J.; Hien, T.T.; Dunstan, S.J. Glucose-6-phosphate dehydrogenase (G6PD) mutations and Haemoglobinuria syndrome in the Vietnamese population. *Malaria J.* **2009**, *8*, 152-160.

Appendix

The numerical successive approximation corresponding to Equations (8–11) as described in the section "Mechanistic Details of Autoxidation of Human HbO$_2$ A: Computer Simulations" was achieved using the Runge–Kutta method by proceeding one-by-one along with the following steps:

Step 1:

$$O\Delta[(\alpha^{2+}\beta^{2+})_2] = -[(\alpha^{2+}\beta^{2+})_2](t) \times (k_1 + k_2)$$

$$P\Delta[(\alpha^{2+}\beta^{2+})_2] = -\{[(\alpha^{2+}\beta^{2+})_2](t) + 1/2 \times \Delta t \times O\Delta[(\alpha^{2+}\beta^{2+})_2]\} \times (k_1 + k_2)$$

$$Q\Delta[(\alpha^{2+}\beta^{2+})_2] = -\{[(\alpha^{2+}\beta^{2+})_2](t) + 1/2 \times \Delta t \times P\Delta[(\alpha^{2+}\beta^{2+})_2]\} \times (k_1 + k_2)$$

$$R\Delta[(\alpha^{2+}\beta^{2+})_2] = -\{[(\alpha^{2+}\beta^{2+})_2](t) + \Delta t \times Q\Delta[(\alpha^{2+}\beta^{2+})_2]\} \times (k_1 + k_2)$$

Step 2:

$$O\Delta[(\alpha^{3+}\beta^{2+})_2] = [(\alpha^{2+}\beta^{2+})_2](t) \times k_1 - [(\alpha^{3+}\beta^{2+})_2](t) \times k_3$$

$$P\Delta[(\alpha^{3+}\beta^{2+})_2] = [(\alpha^{2+}\beta^{2+})_2](t) \times k_1 - \{[(\alpha^{3+}\beta^{2+})_2](t) + 1/2 \times \Delta t \times O\Delta[(\alpha^{3+}\beta^{2+})_2]\} \times k_3$$

$$Q\Delta[(\alpha^{3+}\beta^{2+})_2] = [(\alpha^{2+}\beta^{2+})_2](t) \times k_1 - \{[(\alpha^{3+}\beta^{2+})_2](t) + 1/2 \times \Delta t \times P\Delta[(\alpha^{3+}\beta^{2+})_2]\} \times k_3$$

$$R\Delta[(\alpha^{3+}\beta^{2+})_2] = [(\alpha^{2+}\beta^{2+})_2](t) \times k_1 - \{[(\alpha^{3+}\beta^{2+})_2](t) + \Delta t \times Q\Delta[(\alpha^{3+}\beta^{2+})_2]\} \times k_3$$

Step 3:

$$O\Delta[(\alpha^{2+}\beta^{3+})_2] = [(\alpha^{2+}\beta^{2+})_2](t) \times k_2 - [(\alpha^{2+}\beta^{3+})_2](t) \times k_4$$

$$P\Delta[(\alpha^{2+}\beta^{3+})_2] = [(\alpha^{2+}\beta^{2+})_2](t) \times k_2 - \{[(\alpha^{2+}\beta^{3+})_2](t) + 1/2 \times \Delta t \times O\Delta [(\alpha^{2+}\beta^{3+})_2]\} \times k_4$$

$$Q\Delta[(\alpha^{2+}\beta^{3+})_2] = [(\alpha^{2+}\beta^{2+})_2] (t) \times k_2 - \{[(\alpha^{2+}\beta^{3+})_2](t) + 1/2 \times \Delta t \times P\Delta[(\alpha^{2+}\beta^{3+})_2]\} \times k_4$$

$$R\Delta[(\alpha^{2+}\beta^{3+})_2] = [(\alpha^{2+}\beta^{2+})_2] (t) \times k_2 - \{[(\alpha^{2+}\beta^{3+})_2](t) + \Delta t \times Q\Delta [(\alpha^{2+}\beta^{3+})_2]\} \times k_4$$

Step 4:

$$\Delta[(\alpha^{2+}\beta^{2+})_2] = \Delta t \times 1/6 \times (O\Delta[(\alpha^{2+}\beta^{2+})_2] + 2 \times P\Delta[(\alpha^{2+}\beta^{2+})_2] + 2 \times Q\Delta[(\alpha^{2+}\beta^{2+})_2] + R\Delta[(\alpha^{2+}\beta^{2+})_2])$$

$$\Delta[(\alpha^{3+}\beta^{2+})_2] = \Delta t \times 1/6 \times (O\Delta[(\alpha^{3+}\beta^{2+})_2)] + 2 \times P\Delta[(\alpha^{3+}\beta^{2+}_2)] + 2 \times Q\Delta[(\alpha^{3+}\beta^{2+})_2)] + R\Delta[(\alpha^{3+}\beta^{2+})_2)])$$

$$\Delta[(\alpha^{2+}\beta^{3+})_2] = \Delta t \times 1/6 \times (O\Delta[(\alpha^{2+}\beta^{3+})_2] + 2 \times P\Delta[(\alpha^{2+}\beta^{3+})_2] + 2 \times Q\Delta[(\alpha^{2+}\beta^{3+})_2] + R\Delta[(\alpha^{2+}\beta^{3+})_2])$$

Step 5:

$$[(\alpha^{2+}\beta^{2+})_2](t + \Delta t) = [(\alpha^{2+}\beta^{2+})_2](t) + \Delta[(\alpha^{2+}\beta^{2+})_2]$$

$$[(\alpha^{3+}\beta^{2+})_2](t + \Delta t) = [(\alpha^{3+}\beta^{2+})_2](t) + \Delta[(\alpha^{3+}\beta^{2+})_2]$$

$$[(\alpha^{2+}\beta^{3+})_2](t + \Delta t) = [(\alpha^{2+}\beta^{3+})_2](t) + \Delta[(\alpha^{2+}\beta^{3+})_2]$$

$$[(\alpha^{3+}\beta^{3+})_2] (t + \Delta t) = [\alpha^{2+}\beta^{2+})_2]_{t=0} - [(\alpha^{2+}\beta^{2+})_2](t + \Delta t) - [(\alpha^{3+}\beta^{2+})_2](t + \Delta t) - [(\alpha^{2+}\beta^{3+})_2](t + \Delta t)$$